AD_____

Award Number: W81XWH-06-1-0436

TITLE: Measurement of pO2 and pH in Living Breast Tumor Models with Three-Dimensional Resolution by Multiphoton Microscopy during Combined Therapy with Herceptin

PRINCIPAL INVESTIGATOR: Ryan M Lanning
Rakesh K. Jain, Ph.D.

CONTRACTING ORGANIZATION: Massachusetts Institute of Technology
Cambridge, MA 02139

REPORT DATE: April 2007

TYPE OF REPORT: Annual Summary

PREPARED FOR: U.S. Army Medical Research and Materiel Command
Fort Detrick, Maryland 21702-5012

REPORT DOCUMENTATION PAGE

Form Approved
OMB No. 0704-0188

1. REPORT DATE	2. REPORT TYPE	3. DATES COVERED
01-04-2007	Annual Summary	15 Mar 2006 – 14 Mar 2007

4. TITLE AND SUBTITLE

Measurement of pO2 and pH in Living Breast Tumor Models with Three-Dimensional Resolution by Multiphoton Microscopy during Combined Therapy with Herceptin

5a. CONTRACT NUMBER

5b. GRANT NUMBER
W81XWH-06-1-0436

5c. PROGRAM ELEMENT NUMBER

6. AUTHOR(S)

Ryan M Lanning, Rakesh K. Jain, Ph.D.

Email: ryan@steele.mgh.harvard.edu

5d. PROJECT NUMBER

5e. TASK NUMBER

5f. WORK UNIT NUMBER

7. PERFORMING ORGANIZATION NAME(S) AND ADDRESS(ES)

Massachusetts Institute of Technology
Cambridge, MA 02139

8. PERFORMING ORGANIZATION REPORT NUMBER

9. SPONSORING / MONITORING AGENCY NAME(S) AND ADDRESS(ES)
U.S. Army Medical Research and Materiel Command
Fort Detrick, Maryland 21702-5012

10. SPONSOR/MONITOR'S ACRONYM(S)

11. SPONSOR/MONITOR'S REPORT NUMBER(S)

12. DISTRIBUTION / AVAILABILITY STATEMENT
Approved for Public Release; Distribution Unlimited

13. SUPPLEMENTARY NOTES
Original contains colored plates: ALL DTIC reproductions will be in black and white.

14. ABSTRACT

Multiphoton laser scanning microscopy (MPLSM) has proved to be an important tool in cancer research providing insight into morphologic changes in tumor vasculature, extracellular matrix components and gene expression. However, there is a lack of techniques utilizing multiphoton microscopy to study functional physiologic parameters that are important in tumor development and response to therapy. This report details the development of methods to quantify pO2 and pH in vivo with high three-dimensional resolution (~1 μm3) and significant depth penetration (up to 400 μm) with MPLSM. The technique of phosphorescence quenching microscopy (PQM) was adapted to a multiphoton microscope to permit pO2 measurements using the Pd-porphyrin dendrimer, OxyphorR2 as the oxygen reporter. Measurements of pH were completed using MPLSM and a novel semiconductor nanocrystal (NC)-based reversible, ratiometric pH biosensor exploiting resonance energy transfer from the nanocrystal to a pH sensitive dye.

15. SUBJECT TERMS
Angiogenesis, Multiphoton Laser Scanning Microscopy, Phosphorescence Quenching, Ratiometric Imaging, Hypoxia, pH, Tumor Microenvironment, HER2/neu, Herceptin, Radiotherapy, Taxol

16. SECURITY CLASSIFICATION OF:			17. LIMITATION OF ABSTRACT	18. NUMBER OF PAGES	19a. NAME OF RESPONSIBLE PERSON
a. REPORT	b. ABSTRACT	c. THIS PAGE			USAMRMC
U	U	U	UU	37	19b. TELEPHONE NUMBER *(include area code)*

Table of Contents

Introduction:

This report addresses the developments and key research accomplishments during Year 1 of the Predoctoral Traineeship Award entitled "Measurement of pO_2 and pH in living breast tumor models with three-dimensional resolution by multiphoton microscopy during combined therapy with Herceptin". The overall goal of this project is to rationally schedule combined therapy with Herceptin in murine models of HER2-positive breast cancer by studying relevant functional changes in physiology that occur during therapy. Specifically, further understanding of how tumor microenvironmental oxygen concentration (pO_2) and acidity (pH) may be modulated during targeted breast cancer therapy (Herceptin) due to its anti-angiogenic effects could help enhance the application of radiotherapy and chemotherapy (Taxol), respectively. To achieve the stated research goal, I proposed to develop techniques for measuring *in vivo* pO_2 and pH of HER2-positive and negative primary tumors in murine models of breast cancer using multiphoton laser scanning microscopy (MPLSM). The emphasis of year 1 was to design, develop and implement these techniques using a multiphoton microscope and to quantify *in vivo* pO_2 and pH in an orthotopic murine breast cancer model.

Body:

Year 1 of this training award focused on quantifying *in vivo* pO_2 and pH in breast cancer tumors in the MFP of female SCID mice using multiphoton microscopy. The major goals as outlined in the SOW were i.) develop methods to perform phosphorescence quenching microscopy with MPLSM; ii.) develop methods to measure pH with fluorescence ratiometric imaging (FRIM) using MPLSM; iii.) *in vivo* application of these techniques to chart the progression of the breast cancer microenvironment.

Development of MPLSM-PQM system to quantify pO_2: To measure pO_2, the technique of phosphorescence quenching microscopy (PQM) using the oxygen sensitive porphyrin dendrimer, OxyphorR2,[1] was adapted to MPLSM. Quenching of the phosphorescence decay of porphyrin moieties has been commonly used to measure oxygen in a number of different experimental settings[2]. However, most porphyrin molecules used in phosphorescence quenching experiments demonstrate a negligible two-photon absorption cross-section[3] (not easily excitable by MPLSM) and can act as optical limiters[4] through excitation to higher-order excited states due to the long lifetime of the triplet state from whence phosphorescence occurs. Additionally, the long lifetime of the porphyrin molecule (50-100's μs) means the quantum yield (photons emitted) is distributed over a long period instead of a large burst.

The initial technical challenges that had to be addressed was to find an appropriate excitation wavelength permitting two-photon excitation of OxyphorR2 and a sensitive enough detector to detect the phosphorescence decay. I found that OxyphorR2 could be excited in the range of 800 to 920nm and selected 900nm due to improved depth penetration and decreased tissue photodamage. Excitation at 900nm also exhibited excellent two-photon excitation (Figure1). Ordinary multiphoton microscopy imaging photomultiplier tubes (PMTs) are not sensitive enough to the peak emission wavelengths of OxyphorR2 nor to detect the limited photon counts. I found GaAs (Gallium-Arsenide) PMTs to be an acceptable photon counting detector (quantum efficiency at 690nm ~ 10%) for this purpose. Avalanche photodiodes (APDs) are even more sensitive detectors, QE ~ 70%, at these wavelengths, but have a small detector area (~140 μm), thus requiring the sample to be translated or descanning detection rather than scanning the beam for measurements and epifluorescenct detection. All calibration and *in vivo* data thus far have been taken with a GaAs PMT, though I plan to adapt an APD in the future to potentially speed up the pO_2 measurements by as much as a factor of 7.

The components required for phosphorescence quenching microscopy using OxyphorR2 as the oxygen sensor are easily adapted to MPLSM. Figure 2A illustrates the experimental modifications made to the traditional MPLSM setup. Briefly, an electro-optic modulator (Pockels' Cell, Conoptics) is placed in the excitation pathway of the femtosecond Ti-Sapphire laser. This provides the ability to permit only limited pulses of the excitation light as seen in Figure 2B. The large peak in the raw data is due to the excitation pulse, while the decay occurs when no excitation light is applied to the sample. Custom-built electronics and Labview software are used to drive the Pockels' cell and collect data. The scan box (Olympus Flouview 300) parks the

laser beam and a 20X 0.95NA objective is used to both excite the porphyrin and collect the phosphorescence. A sensitive photon counting detector (GaAs PMT) is placed in the epifluorescence emission pathway with an appropriate bandpass filter centered on the phosphorescence emission. Shortpass filters can also be used to further limit the scattered excitation laser light from reaching the detector. The electronic pulses from the PMT are then binned to build a photon counting histogram using a multichannel scaler (SR430, Stanford Research Systems). The raw data is then fit to a single or multi-exponential decay (Figure 2C, D). Imaging of the sample can also be performed with this setup using other imaging detectors located in the emission path below the phosphorescence detector. Depending on sample type, reporter molecule concentrations, and excitation power a single pO_2 measurement can take anywhere from 0.5 – 3 seconds.

To obtain quantitative values for oxygen concentration, pO_2, the oxygen sensor must be calibrated. The interaction between phosphorescence lifetime of the porphyrin and pO_2 is known as the Stern-Volmer relationship. The Stern-Volmer relationship is defined by a given quenching constant and lifetime of the oxygen sensitive phosphor at zero pO_2 (known as τ_0). Typically, this relationship is found by linearly fitting the inverse of the lifetime at different oxygen concentrations.[5] The Stern-Volmer relationship is due to a bi-molecular quenching reaction between the excited triplet state of the porphyrin and oxygen molecules. Anything that interferes with this bi-molecular reaction, such as binding to proteins, can affect the lifetime of the phosphor and thus the quenching constant and τ_0. Therefore, oxygen calibrations must be performed in solutions with the appropriate percent-weight of albumin for *in vivo* measurements. It has been reported that for the OxyphorR2 sensor this process is saturated at albumin concentrations found *in vivo* (~ 2-4%).[5]

To perform calibration of the oxygen sensor using MPLSM-PQM, I designed an air-tight recirculation system. The calibration setup employs a peristaltic pump and fiber oxygenator to modulate the pO_2 of a circulating solution of porphyrin in PBS with or without BSA. An oxygen-impermeable quartz flow-cell with <0.5mm walls permits excitation of the porphyrin solution by MPLSM-PQM. Independent measurements of pO_2 are obtained by the FOXY fiber-optic oxygen sensor (Ocean Optics) placed in a custom-built reservoir in the recirculation system. Additionally, known mixes of oxygen and nitrogen are applied to the oxygenator. All interconnected tubing is gas-impermeable Tygon tubing.

As described in the literature the effect of albumin is saturated between 2-4% by-weight in solution. [5] Ionic content and pH have very little effect on the Stern-Volmer relationship for OxyphorR2. Temperature does have a profound effect on the phosphor lifetime because quenching increases with rising temperature. Excitation wavelengths below 875nm also appear to have an effect on the Stern-Volmer relationship, though it is unclear if this is due to the sensitivity of the detector to shorter excitation wavelengths or unknown photophysical processes. Therefore, all calibration for *in vivo* work should be carried out at 37°C, 4% albumin and at the given excitation wavelength. Figure 3 illustrates the Stern-Volmer relationship for OxyphorR2 at room temperature (25°C) with the quenching constant (k_q) and τ_0 comparable to previous reports.[5]

Development of MPLSM-FRIM system to quantify pH: The original objective of the proposal as outlined in the SOW was to utilize fluorescence ratiometric imaging of BCECF [6] or 2,3-dicyanohydroquinone (DCHQ) [7] to quantify *in vivo* pH. However, BCECF could not be used as a ratiometric fluorescent probe of pH because the acid and base forms of the molecule do not have an excitation wavelength where their two-photon absorption cross-sections are equal. This means that one form will always dominate the fluorescence emission making ratiometric imaging untenable. DCHQ, an adequate ratiometric pH sensor that has been demonstrated with two-photon excitation[7], could prove toxic to living animals and thus should be encapsulated in liposomes for *in vivo* use. To surmount these obstacles and develop an ideal ratiometric probe to measure *in vivo* pH using MPLSM, I have been collaborating with the Bawendi and Nocera groups at MIT on the use of Förster Resonance Energy Transfer (FRET) -based ratiometric pH probes utilizing semiconductor nanocrystals (NCs, also know as quantum dots).

A brief background on semiconductor nanocrystals illustrates their significance as the basis for a pH biosensor for multiphoton microscopy: NC's are increasingly used in biological research as fluorescent tracers in microscopy [8, 9], imaging molecular targets [10], cell tracking [11, 12], and sensing [13]. NCs are well suited for

biological imaging with MPLSM due to their intrinsic characteristics: high quantum yield, photostability, narrow photoluminescence peak, and broad excitation spectra [14]. NCs have proven reliable fluorescent markers for multicolor simultaneous imaging in vivo because of an unparalleled two-photon excitation cross-section. [15]

Recent work has shown promise for NCs - acting as donors in FRET - to construct sensing modalities [16] including those for biological analytes such as maltose [17]. Linking a NC to an environmentally sensitive fluorescent dye in which there is a donor-acceptor FRET relationship allows for ratiometric spectral comparison (via modulation of energy transfer or dye emission lifetime/intensity) dependent upon analyte concentration [18] (see Snee *et al*. J. Am. Chem. Soc. 2006, Appendix B). With judicious dye selection, so that there is limited direct excitation, a reversible internally calibrated ratiometric biosensor is possible due to the photostability and environmental insensitivity of the NC. The entire construct inherits the broad excitation spectrum and large two-photon excitation cross-section of the NC – highly desirable attributes for use in vivo with MPLSM. The ratiometric FRET-based NC biosensors I am applying to measure *in vivo* pH are significant in that they are reversible and self-referencing, an innovation over previous designs [19] (see Somers *et al*. Chem. Soc. Rev. 2007, Appendix B).

Initial work by the Nocera and Bawendi groups on a pH sensitive squaraine dye linked to an NC core allowed for self-referenced pH sensing [18]. This complex had a pKa that was too basic (~ 8.8) for in vivo measurements. Additionally, the coupling mechanism between the NC core and dye molecule was based on ester bonds, which can be easily hydrolyzed in the circulation. Building on this work in a collaborative effort, we have developed a pH biosensor that is a NC core conjugated to carboxy SNARF-5F, a pH sensitive dye with a pKa ~ 7.2 [20]. The NC-SNARF construct also utilizes amide bonds for coupling NC to dye. The NC-biosensor has a two photon action cross-section that mirrors that of free NC indicating that the emission of the dye is due to FRET and not direct excitation (Figure 4).

Initial characterization (including *in vivo*) and calibration measurements of the NC-biosensor were carried out by collecting the emission spectra during MPLSM. Briefly, the epifluorescence emission light was coupled into a fiber bundle, which illuminated the slit of a spectrograph with a high-sensitivity CCD detector (Shamrock/Newton, Andor) Calibration of the pH biosensor was performed in phosphate buffers containing 4% bovine serum albumin (BSA) from pH 6 to 8 at 37°C. The introduction of BSA explores the effect of scattering media and potential binding on the ratiometric emission of the pH biosensor. Figure 5 shows the normalized emission spectra and calibration curve based upon ratio of the SNARF to NC peak emission. Similar results can also be obtained using a dichroic filter at the isosbestic point (~585nm) of the construct and imaging with two PMTs employing appropriate bandpass filters to separately integrate the emission from the dot and dye. This suggests the ease at which *in vivo* measurements may be made by ratiometric imaging.

Development and usage of this new NC pH biosensor coupled with technical issues regarding attempts to use the proposed ratiometric pH sensors has led to a deviation in the two-photon pH sensor portion of the SOW and added slight delay of approximately 3 months. *The adjustment to the SOW only regards the pH sensor applied for measuring in vivo pH and not the overall Aims.* Furthermore, the NC-based pH biosensor provides both a powerful new tool for *in vivo* imaging and is fully compatible with the MPLSM pO_2 technique permitting simultaneous measurements.

<u>*In vivo* application of MPLSM-PQM and NC-biosensor in murine models of breast cancer</u>:

Animal Model – Chronic window MFP chamber – The chronic window chamber model implanted on the MFP of female mice (Figure 6) permits continuous observation of orthotopic breast cancer during tumor progression and treatment. The surgery is relatively simple and takes 25-30 minutes per mouse for chamber implantation. Briefly, the mouse is shaved and denuded midline to midline over the area of MFP #3. The #3 nipple is used as a marker to create a flap containing the MFP, superficial epigastric vein and mammary artery. The back half of the titanium chamber is then sutured onto the flap. The tissue around the lower screws is resected to allow penetration to the front side of the chamber. The front half of the titanium chamber is temporarily placed and used to outline the area of skin for the window. The skin, fat and some subcutaneous muscle is carefully dissected away to expose the MFP. The front of the chamber with cover glass is placed in position, screwed

down and sutured in place. The cell lines used in this study (MDA-MB-361HK and MDA-MD-231) can both be implanted after chamber placement and allowed to grow. To determine if chamber placement is possible after tumor implantation, tumor cells (~2M) were injected subcutaneously beneath the #3 nipple and allowed to grow to 2 - 5 mm in diameter. Successful chamber placement was possible in all cases, which suggests that chamber placement will be possible on spontaneous mammary carcinomas, such as the PyMT-MMTV mouse [21], around the #2 and #3 MFPs.

In vivo pO_2 measurements – An initial obstacle to the application of MPLSM-PQM with OxyphorR2 in living tumors implanted in the murine MFP chamber model was the delivery of the oxygen sensor to the interstitium. I attempted three methods to introduce the phosphor into the tumor. The ideal delivery method is intravenously through the tail vein of the mouse. To accomplish this, OxyphorR2 dissolved in PBS was given i.v. through the dorsal tail vein at a dosage of 65-100mg/kg. At these dosages, very little signal in the interstitium was detectable within the first hour after administration. If more time is allowed to pass, additional phosphor diffuses into the interstitium. I found that twenty-four to forty-eight hours after i.v. injection provide the best signal throughout the tumor suggesting the phosphor had broadly diffused. I even discovered that in many cases it is possible to measure pO_2 up to 36 hours after the initial injection, suggesting repeatable measurements are possible without additional injections. It is important to note that because pO_2 measurements with PQM are based on lifetime and not intensity, the phosphor is not required to have uniform distribution within the interstitium. The two other methods of administration involve directly applying the phosphor to the tumor through superfusion or microinjection. Both methods permit the use of much more dilute concentrations of phosphor, but also disturb the tumor microenvironment through removal of the cover glass or insertion of a micropipette into the tumor. With all three cases of administration, equivalent pO_2 values are obtained in similar tumor models. For "normal" mock-implanted chambers, superfusion is often the method of choice due to decreased extravasation of the phosphor into normal interstitium.

In vivo measurements of pO_2 are taken with the MPLSM-PQM instrument described above using the range of excitation powers presented in Figure 1 to ensure two-photon excitation at 900nm. OxyphorR2 (65-100mg/kg) dissolved in PBS is injected i.v. twenty-four hours before imaging. Just prior to imaging, 0.1 ml of a mixture containing 10mg/ml OxyphorR2 and 8 mg/ml FITC-dextran 2M is injected i.v. to permit intravascular pO_2 measurements and imaging of vascular morphology, respectively. The laser beam is then parked at various locations throughout the tumor to measure both intravascular and interstitial pO_2 as well as three-dimensioanl pO_2 profiles around blood vessels. The technique exhibited improved depth penetration (up to 400 μm) in comparison to single-photon PQM.

Intravascular measurements demonstrated pO_2 values similar to those presented in the literature for the appropriate vessel sizes. Figure 7 contains a table of average intravascular pO_2 values for two different types of vessels and an image of capillaries in a mock-transplanted chamber. These values compare favorably to those previously reported in the literature [22]. One potential issue concerning intravascular measurements is the distance an excited porphyrin molecule may travel in the vessel before being quenching by oxygen or emitting a photon. For typical pO_2 values (15-80 torr), a porphyrin molecule may travel up to 200 microns in a vessel before phosphorescing or colliding with oxygen. However, the lower the pO_2 is in a vessel in peripheral tissue, the slower the flow. For measurements in the interstitium the porphyrin molecule does not diffuse fast enough on average to exit the two-photon excitation spot suggesting the resolution for pO_2 measurements is on the order of the multiphoton microscope. In a model of murine mammary carcinoma (MCaIV), the tumor blood vessels display a lack of heterogeneity in vessels with diameters lest than 50 μm (Figure 8). This suggests that intravascular measurements alone are not enough to understand the functional dynamics of the tumor vasculature.

Initially, it was very difficult to perform interstitial measurements of pO_2 due to limited extravasation of the phosphor into the interstitium. However, by injecting 24 hours in advance enough phosphor diffuses throughout the interstitium to perform pO_2 measurements. Comparing radial profiles in tumors and normal tissue a number of differences are obvious (Figure 9). The average pO_2 in both the tumor blood vessels and interstitium is lower than that in normal tissue. It is also advantageous to examine the axial and radial profiles

on the same vessel, which is not easily possible without MPLSM-PQM. Figure 10 demonstrates how different the radial and axial profiles can be for a given vessel in a tumor. This suggests that the three-dimensional profile of a tumor vessel is far more complex than the Krogh cylinder model [23] can describe.

Using phosphorescence quenching, OxyphorR2 may be able to quantify relative amounts of protein in the tumor interstitium. The majority of *in vivo* interstitial measurements exhibit a multicomponent decay including both a fast and slow decay. The slow decay is typically 70-100% of the emitted phosphorescence in a given measurement and permits statistically adequate fitting of the data by a single-exponential decay as seen in the residuals. However, further understanding of the fast component fraction, which is most likely freely diffusing, may lead to methods for quantifying proteins that bind to the phosphor. This is certainly a research topic worth pursuing as it would add additional functional data about the tumor microenvironment.

In vivo pH measurements – The application of the NC-based pH biosensor has been hampered by biofouling *in vivo*. Essentially, many of the coatings used to prepare the NCs to be soluble and attach to SNARF demonstrate non-specific binding to intravascular cells and endothelium. This meant that not enough pH biosensor could extravasate into the tumor interstitium even if the hydrodynamic radius of the construct was relatively small (< 5nm). Even with direct intratumoral injection, binding of the pH biosensor to extracellular matrix components was still observed. However, it was still possible to measure intravascular pH (Figure 11). With my collaborators from the Bawendi and Nocera groups, we explored different types (quantomer, dendrimer, and PEGylation) and charges (100% amine, 100% hydroxyl group or a mix). From our studies we found that the amino-PEGylated constructs did not bind *in vivo* (Figure 12) and extravasated to a large extent from the tumor vasculature within a couple hours. The *in vitro* data given above was completed using amino-PEGylated NC pH biosensor constructs. The various constructs listed above have also been tested over a period of 3 months for toxicity in mice and none has yet been observed. We are now synthesizing more of this construct and will be performing *in vivo* measurements as outlined in the Statement of Work.

Breast Cancer Training Program: With respect to the longitudinal clinic and coursework described in the proposed breast cancer training program, I completed both a clinical course in the MGH Department of Radiation Oncology on radiation biology as it pertains to clinical treatment and a course at MIT entitled "Magnetic Resonance Analytic, Biochemical and Imaging Techniques". I also taught 3 sections in the Steele Lab for Tumor Biology laboratory course: Light Microscopy, Fluorescence Recovery After Photobleaching (techniques to measure *in vivo* macromolecular diffusion), and Multiphoton Microscopy. As part of my research program during this past year, I built a new multiphoton laser scanning microscope and incorporated the components for performing pO_2 measurements and a spectrometer for multispectral imaging. In Year 2, I will begin shadowing physicians in the breast clinic and will also participate as a research assistant in a clinical study on breast cancer as part of my training in the Medical Engineering and Medical Physics graduate program at MIT.

Key Research Accomplishments:

- Developed a MPLSM-PQM system for quantifying oxygen concentration (pO_2)
- Adapted MPLSM-PQM technique to models of breast cancer to measure *in vivo* pO_2
- Identified three-dimensional pO_2 profiles from tumor vessels as the most informative functional parameter versus random intravascular measurements
- Developed and calibrated a novel semiconductor nanocrystal-based pH biosensor using MPSLM
- Implemented the mammary fat pad chamber model on female mice with pre-implanted tumors, suggesting that the chamber should work with spontaneous models of murine breast cancer.

Reportable Outcomes:

No reportable outcomes at this time as defined by the reporting procedures.
Paper is in preparation regarding quantifying *in vivo* tumor pO_2 using MPLSM.
Paper is in preparation regarding NC-based *in vivo* biosensor for quantifying tumor pH.

Conclusion:

The goals of the 1st year of this project were to develop techniques to quantify pO_2 and pH using multiphoton microscopy and apply these methods to study the *in vivo* tumor microenvironment in an orthotopic murine model of breast cancer.

The adaptation of phosphorescence quenching microscopy to the MPLSM has resulted in the ability to quantify *in vivo* pO_2 intravascularly and measure three-dimensional oxygen profiles around vessels. The higher resolution (~ $1\mu m^3$) and significant depth penetration (up to 400μm) is a major improvement over single-photon PQM and invasive microelectrode methods. The measurement speed is slower than ideal (0.5 to 3 seconds per point), but may be improved with a more sensitive optical detector. Future plans for optimizing multiphoton PQM include using a high-sensitivity avalanche photodiode detector and a motorized XYZ stage for quickly scanning three-dimensional profiles around vessels.

Development of pH sensitive ratiometric imaging with MPLSM using commercially available optical pH indicators proved difficult due to unbalanced two-photon excitation between the acid and base forms (BCECF) or potential toxicity (DHCQ). To overcome this problem, a reversible, internally calibrated ratiometric pH biosensor based on FRET between a semiconductor nanocrystal and pH-sensitive dye has been developed and applied to multiphoton microscopy with encouraging results. As described, the NC pH biosensor demonstrates ideal optical properties for imaging with MPLSM. However, *in vivo* work has been hampered due to biocompatibility issues of the solublilizing coating of NC-construct causing non-specific binding and limited extravasation into the interstitial space. Amino-PEGylating the NCs and utilizing amide bonds for attachment of the pH sensitive dye vastly improved the pH biosensor biocompatibility and diffusion into the tumor interstitium. This pH biosensor will soon be combined with pO_2 measurements with the MPLSM to complete the tasks of measuring pO_2 and pH in the tumor microenvironment of HER2-positive and negative breast cancer during tumor progression in the MFP chamber model.

Both the pO_2 and NC-based pH biosensor techniques utilizing MPLSM are important additional tools for further understanding preclinical translational research models of breast cancer. Application of these techniques to further our understanding of functional changes in tumor physiology during different treatment regimens may help us more rationally design treatment programs in the clinic. Independently, pO_2 measurements with a porphyrin moiety have demonstrated that it is possible to utilize porphyrin molecules with MPLSM. This could prove useful for individuals studying targeted photodynamic therapy which often uses porphyrin-based molecules as the source of cytotoxic free-radicals in cancer treatment. Furthermore, evidence of the use of FRET-based NC biosensors for pH demonstrates proof-of-principle that other NC-based biosensors for different analytes (calcium, oxygen, sodium, glucose, etc) may be easily achievable.

References:

1. Lo L-W, Vinogradov SA, Koch CJ and Wilson DF (1997). A new, water soluble, phosphor for oxygen measurements in vivo. *Adv. Exptl. Med. Biol*. **428**: 651-6.
2. Papkovsky DB and O'Riordan TC (2005). Emerging applications of phosphorescent metalloporphyrins. *J. Fluorescence*. 15: 569-84.
3. Brinas RP, Troxler T, Hochstrasser RM, Vinogradov SA (2005). Phosphorescent oxygen sensor with dendritic protection and two-photon absorbing antenna. *J Am. Chem. Soc.* 127: 11851-62.

4. Dou K, Sun X, Wang X, Parkhill R, Guo Y, and Knobbe ET (1999). Optical limiting and nonlinear absorption of excited states in metalloporphyrin-doped sol gels. *IEEE J. Quantum Elec.* **35**: 1004-14.
5. Lo L-W, Vinogradov SA, Koch CJ and Wilson DF (1997). A new, water soluble, phosphor for oxygen measurements in vivo. *Adv. Exptl. Med. Biol*. **428**: 651-6.
6. Helmlinger G, Yuan F, Dellian M and Jain RK (1997). Interstitial pH and pO_2 gradients in solid tumors *in vivo*: high-resolution measurements reveal a lack of correlation. *Nat. Med.* **3**: 177-82.
7. Jobsis PD, Combs CA, and Balaban, RS (2005). Two-photon excitation fluorescence pH detection using 2,3-dicyanohydroquinone: a spectral ratiometric approach. *J. Microscopy*. **217**: 260-4.
8. Dubertret B, Skourides P, Norris D J, Noireaux V, Brivanlou AH and Libchaber A (2002). In vivo imaging of quantum dots encapsulated in phospholipid micelles. *Science*. **298**: 1759-1762.
9. Jain RK and Stroh M. (2004) Zooming in and out with quantum dots. *Nat Biotechnol*. **22**: 959-960.
10. Wu XY, Liu HJ, Liu JQ, Haley KN, Treadway JA, Larson JP, Ge NF, Peale F and Bruchez MP (2003). Immunofluorescent labeling of cancer marker Her2 and other cellular targets with semiconductor quantum dots. *Nat Biotechnol*. **21**: 41-46.
11. Gao X, Cui Y, Levenson RM, Chung LW, and Nie S (2004). In vivo cancer targeting and imaging with semiconductor quantum dots. *Nat Biotechnol*. **22**: 969-976.
12. Michalet X, Pinaud FF, Bentolila LA, Tsay JM, Doose S, Li JJ, Sundaresan G, Wu AM, Gambhir SS and Weiss S (2005). Quantum dots for live cells, in vivo imaging, and diagnostics. *Science*. **307**: 538-544.
13. Medintz IL, Uyeda HT, Goldman ER and Mattoussi H (2005). Quantum dot bioconjugates for imaging, labeling and sensing. *Nat Mater*. **4**: 435-446.
14. Chan WC, Maxwell DJ, Gao X, Bailey RE, Han M and Nie S (2002). Luminescent quantum dots for multiplexed biological detection and imaging. *Curr. Opin. Biotechnol.* **13**: 40-46.
15. Larson DR, Zipfel WR, Williams RM, Clark SW, Bruchez MP, Wise FW, and Webb WW (2003). Water-soluble quantum dots for multiphoton fluorescence imaging in vivo. *Science*. **300**: 1434-1436.
16. Clapp AR, Medintz IL, Mauro JM, Fisher BR, Bawendi MG and Mattoussi H (2004). Fluorescence resonance energy transfer between quantum dot donors and dye-labeled protein acceptors. *J Am Chem Soc.* **126**: 301-310.
17. Medintz IL, Clapp AR, Mattoussi H, Goldman ER, Fisher B and Mauro JM (2003). Self-assembled nanoscale biosensors based on quantum dot FRET donors. *Nat Mater*. **2**: 630-638.
18. Snee PT, Somers RC, Zimmer JP, Nair GP, Bawendi MG and Nocera DG (2006). A ratiometric CdSe/ZnS nanocrystal pH sensor.*J. Am. Chem. Soc.* **128**: 13320-1.
19. Somers RC, Bawendi MG and Nocera DG (2007). CdSe nanocrystal based chem-/bio- sensors. *Chem. Soc. Rev.* **36**: 579-91.
20. Liu J, Diwu Z and Leung WY (2001). Synthesis and photophysical properties of new fluorinated benzo[c]xanthene dyes as intracellular pH indicators. *Bioorg Med Chem Lett*. **11**: 2903-2905.
21. Lin EY, Jones JG, Li P, Zhu L, Whitney KD, Muller WJ and Pollard JW (2003). Progression to malignancy in the polyoma middle T oncoprotein mouse breast cancer model provides a reliable model for human diseases. Am. J. Pathol. 163: 2113-26
22. Intaglietta M, Johnson PC, Winslow RM (1996). Microvascular and tissue oxygen distribution. *Cardiovasc. Res.* **32**: 632-43.
23. Krogh A (1929). The Anatomy and Physiology of Capillaries. New Haven, United States: Yale University Press.

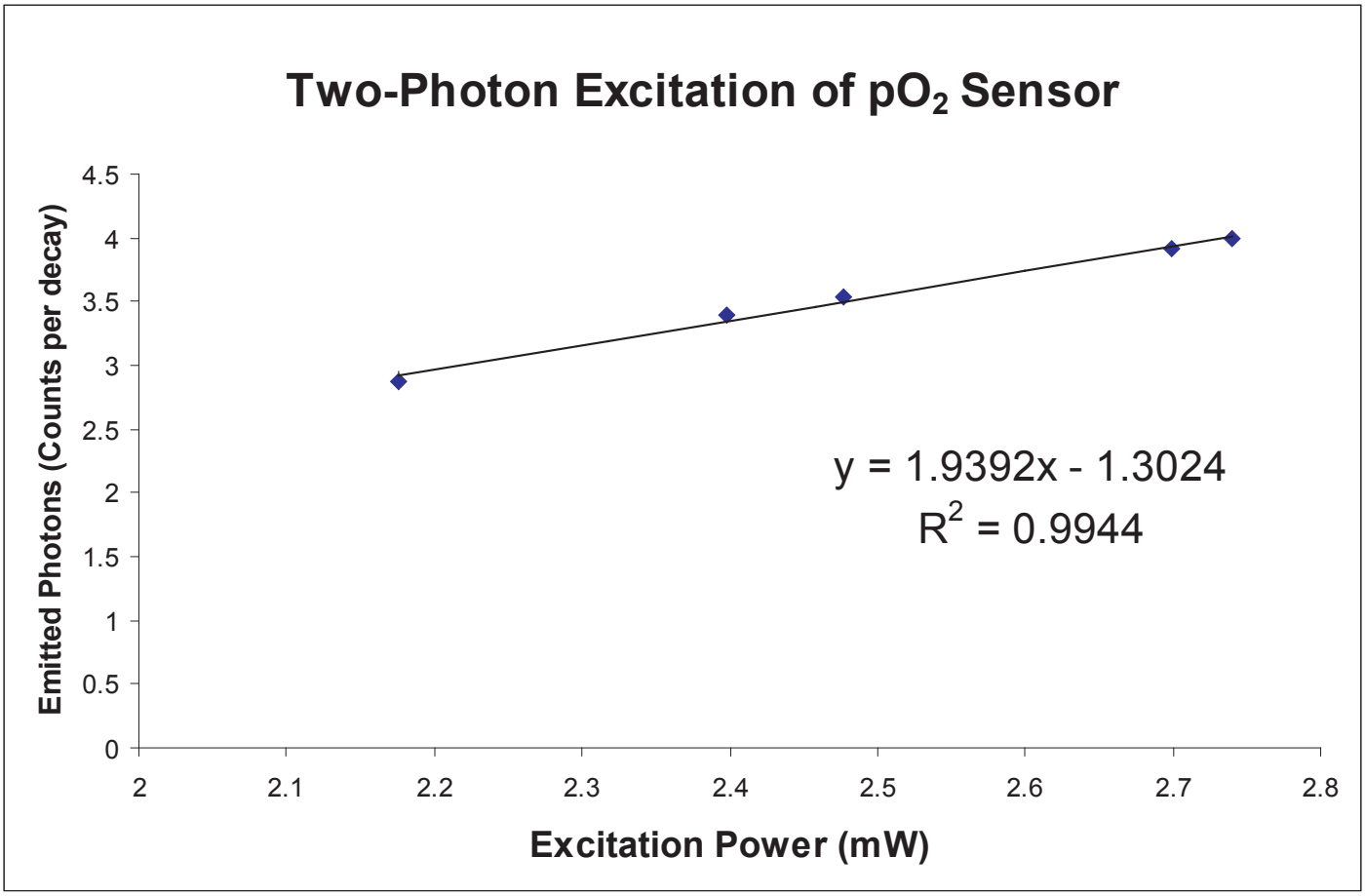

Figure 1: Nonlinear excitation of the porphyrin oxygen sensor using 900nm excitation light from the femtosecond laser source. A slope of 2 in a log-log plot of emitted photons versus excitation power indicates two-photon absorption by a molecule during the excitation from the ground state.

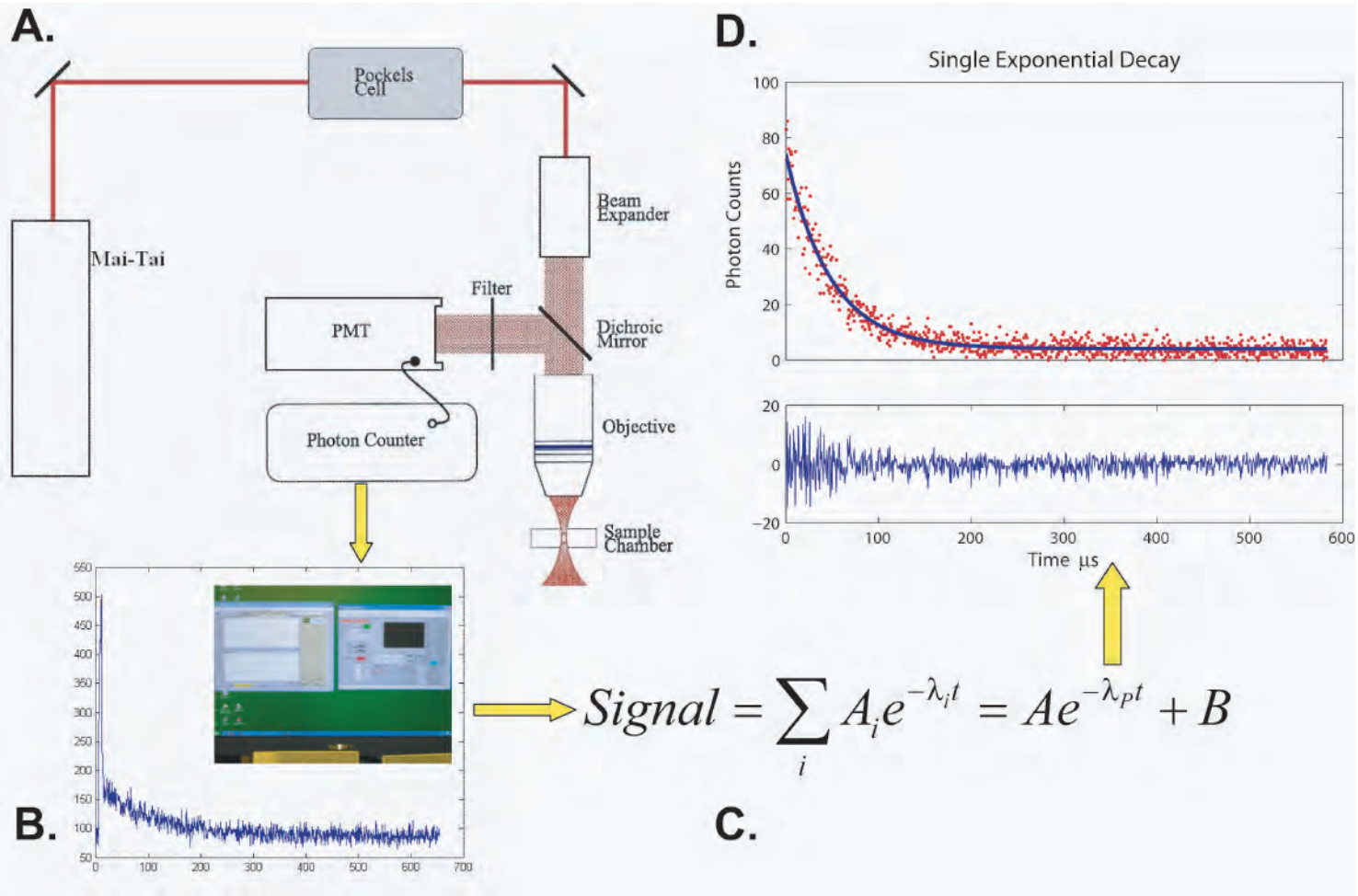

Figure 2: MPLSM-PQM Setup and Data Acquisition – A.) Experimental modifications of MPLSM. B.) Raw data collected from photon counter C.) Signal fit to single or multi-component exponential decay D.) Processed phosphorescence decay data and fit.

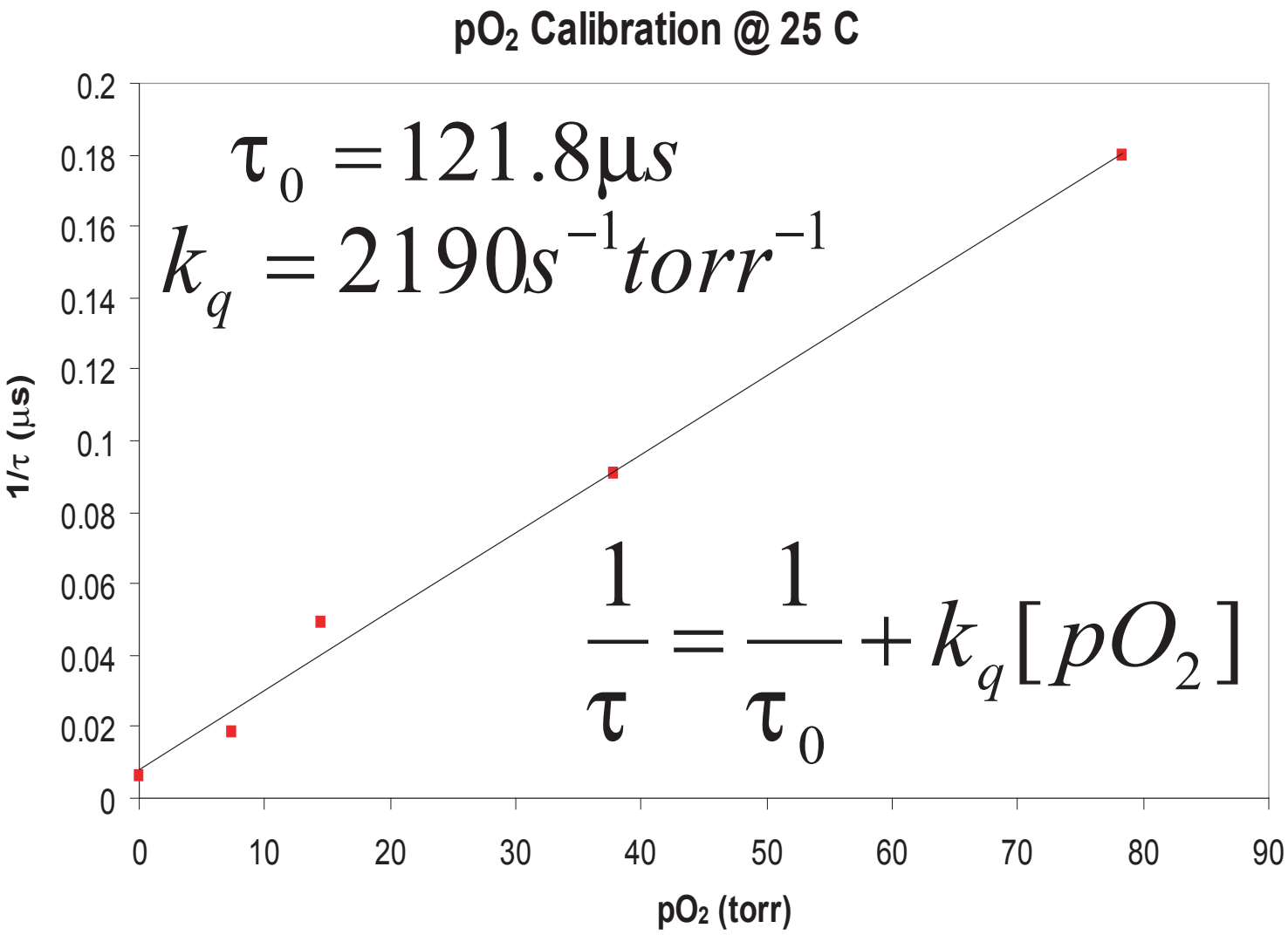

Figure 3: Calibration of OxyphorR2 using MPLSM-PQM at 900nm excitation. The linear Stern-Volmer relationship is given in the lower right. The τ_0 and quenching constant (k_q) are listed for the given linear fit.

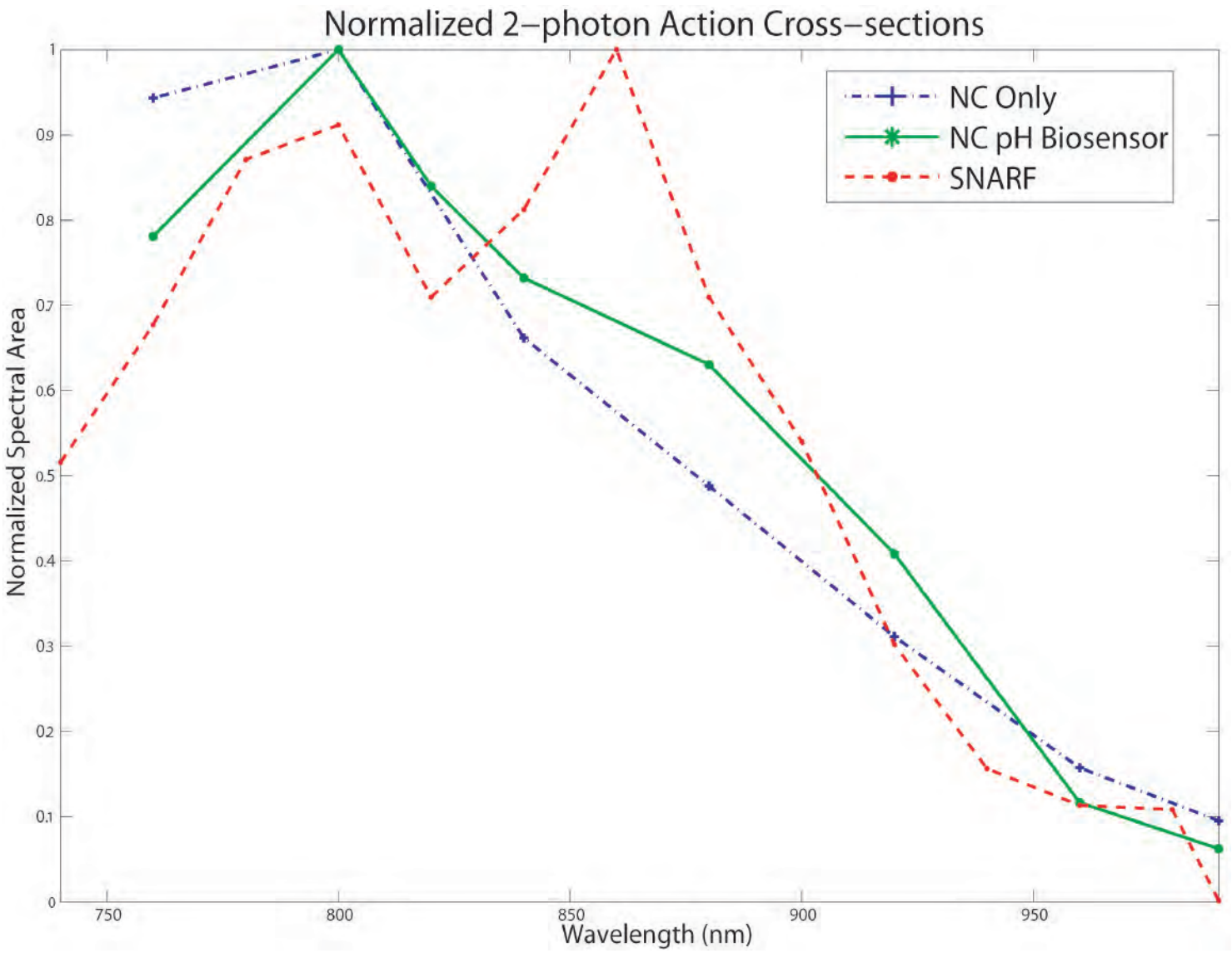

Figure 4: Two-photon action cross-sections of FRET-based NC-SNARF pH Biosensor – The action-cross section of a molecule is a relative measure of the excitation spectrum for MPLSM. In this case all cross-sections are normalized to their maximum to highlight the similarities and differences between the profiles. It is apparent that the NC only and NC pH biosensor have share the same form, while that of the SNARF alone has a large peak around 850nm. It should be noted that the actual values of the cross-section are much larger for the NC and NC biosensor than that of SNARF.

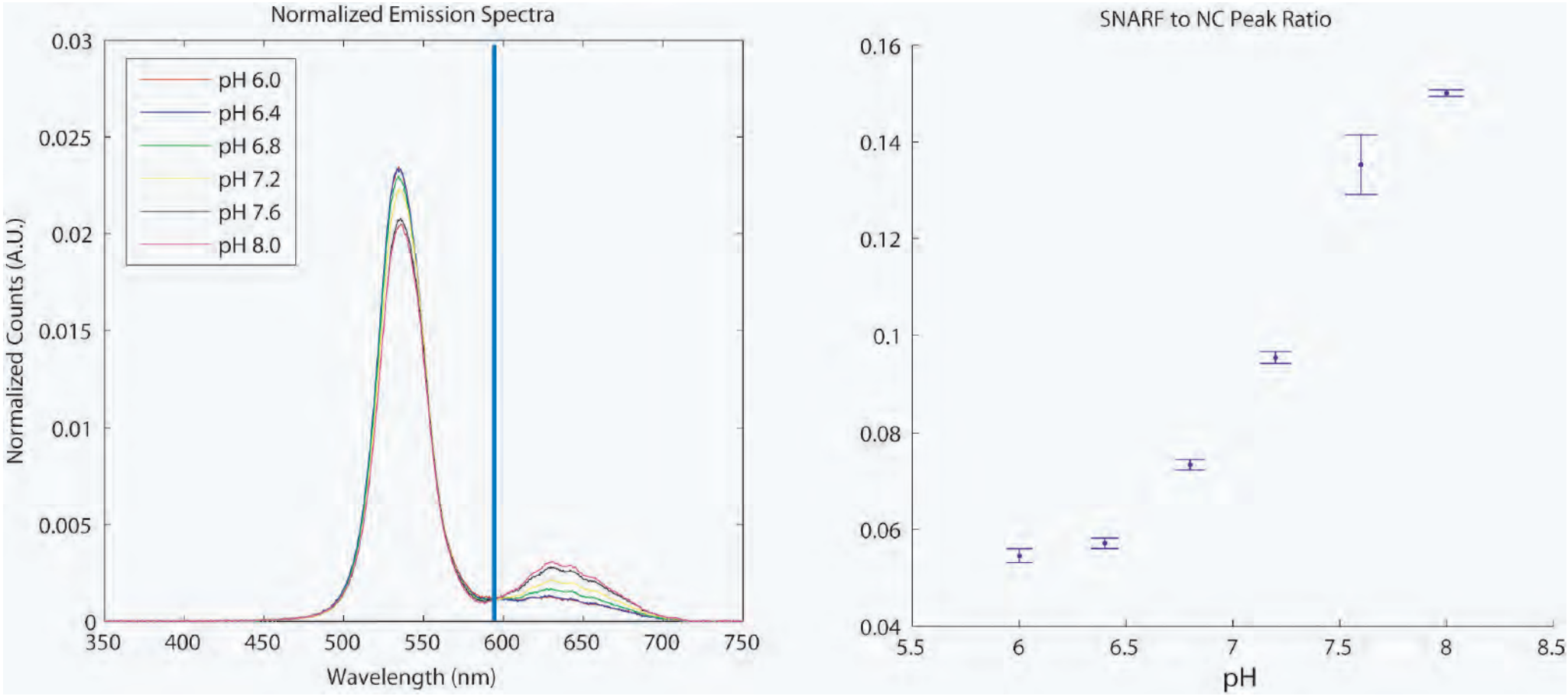

Figure 5: The left portion of this figure shows the normalized emission spectra of the NC-SNARF pH biosensor due to excitation by multiphoton microscopy. The light blue line indicates the isosbestic point and the location at which a dichroic can be placed to permit imaging calibration using two PMTs. The right-hand plot demonstrates a calibration curve for the pH biosensor based on the ratio of the SNARF peak emission to that of the NC. Note that it appears very similar in nature to an acid/base titration curve and that the pKa is ~ 7.2 – close to that of free SNARF. Each point is an average of 3 measurements.

Figure 6: Mammary fat pad chronic window chamber model on a female SCID mouse with a MDA-MB-231 tumor growing orthotopically.

Normal Murine Vascular Network

Vessel	Mean pO_2
Artery (A3)	**49.65**±24.47
Capillary 1 (8 μm)	**14.41**±1.66
Capillary 2 (10 μm)	**19.08**±8.68
Capillary 3 (8 μm)	**22.97**±0.80

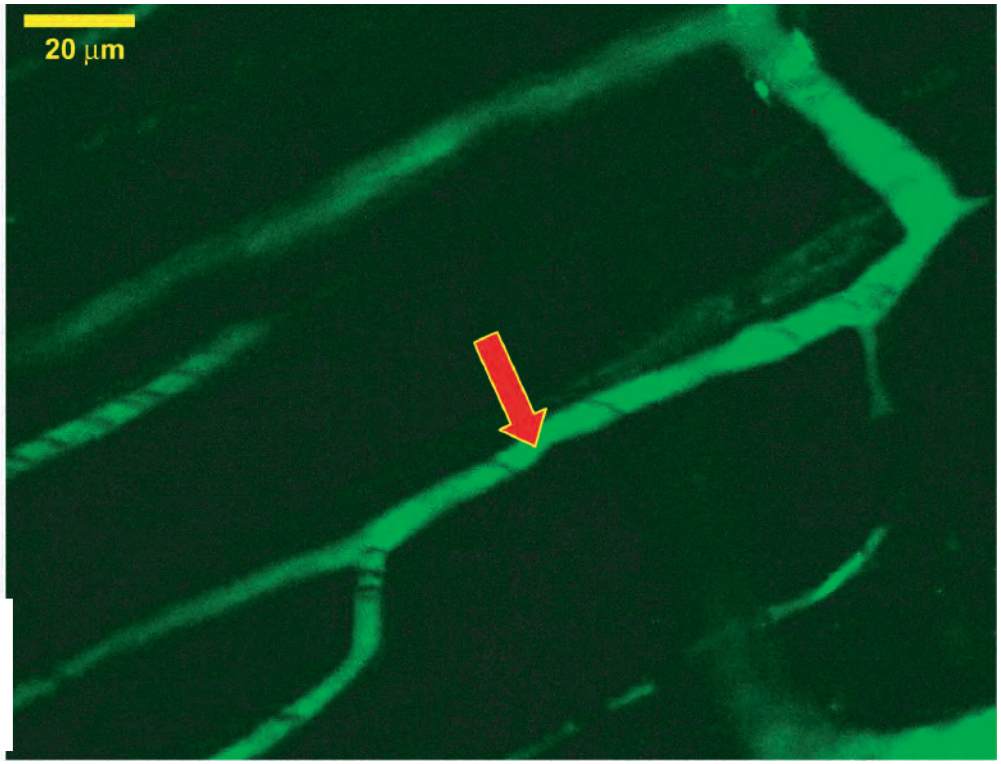

Figure 7: Table illustrating the mean pO_2 in torr in normal blood vessels in the murine chamber models. The image shows a normal capillary network and an 8 μm capillary (red arrow). The shadows of RBCs are visible flowing through this vessek.

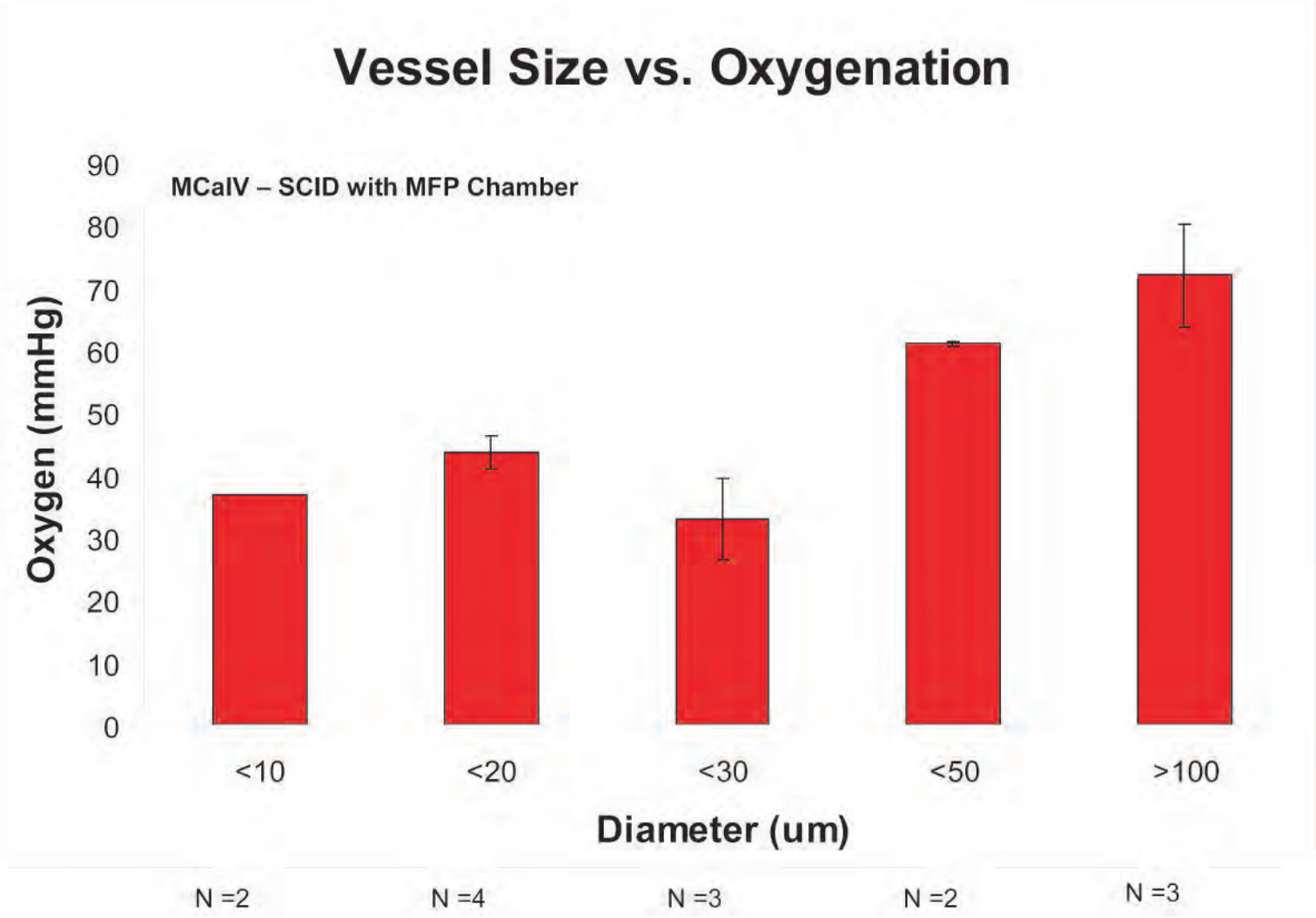

Figure 8: Chart showing the distribution of pO_2 values in the tumor vesseles of a murine mammary carcinoma (MCaIV) implanted in the MFP chamber.

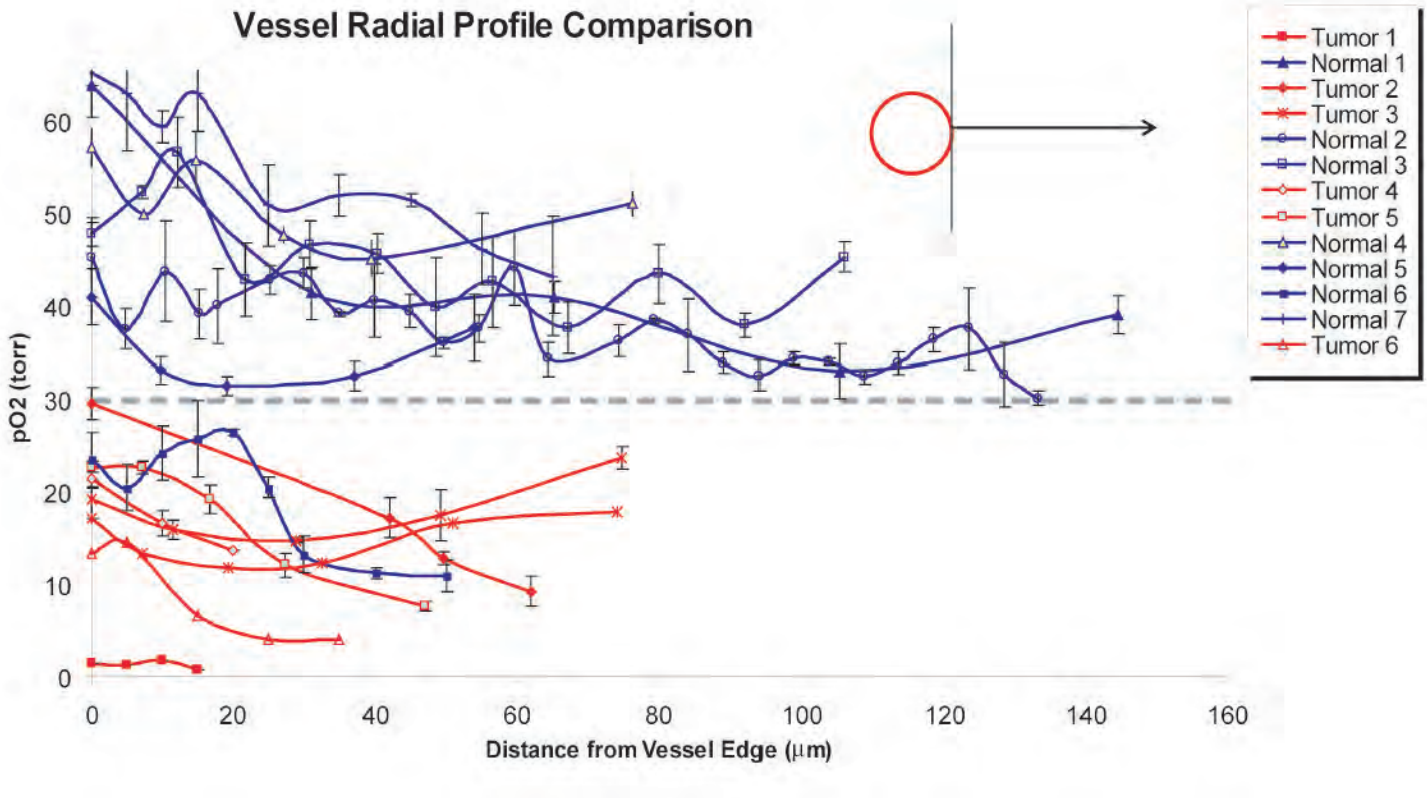

Figure 9: Radial oxygen profiles as measured by MPLSM-PQM from randomly selected vessels in tumors and mock-transplanted chambers.. Blue – normal chamber vessels. Red – tumor vessels. The dashed line delineates a functional separation between the two groups of vessels. The diagram in the upper right of the plot inidicates the direction of measurement for the profiles.

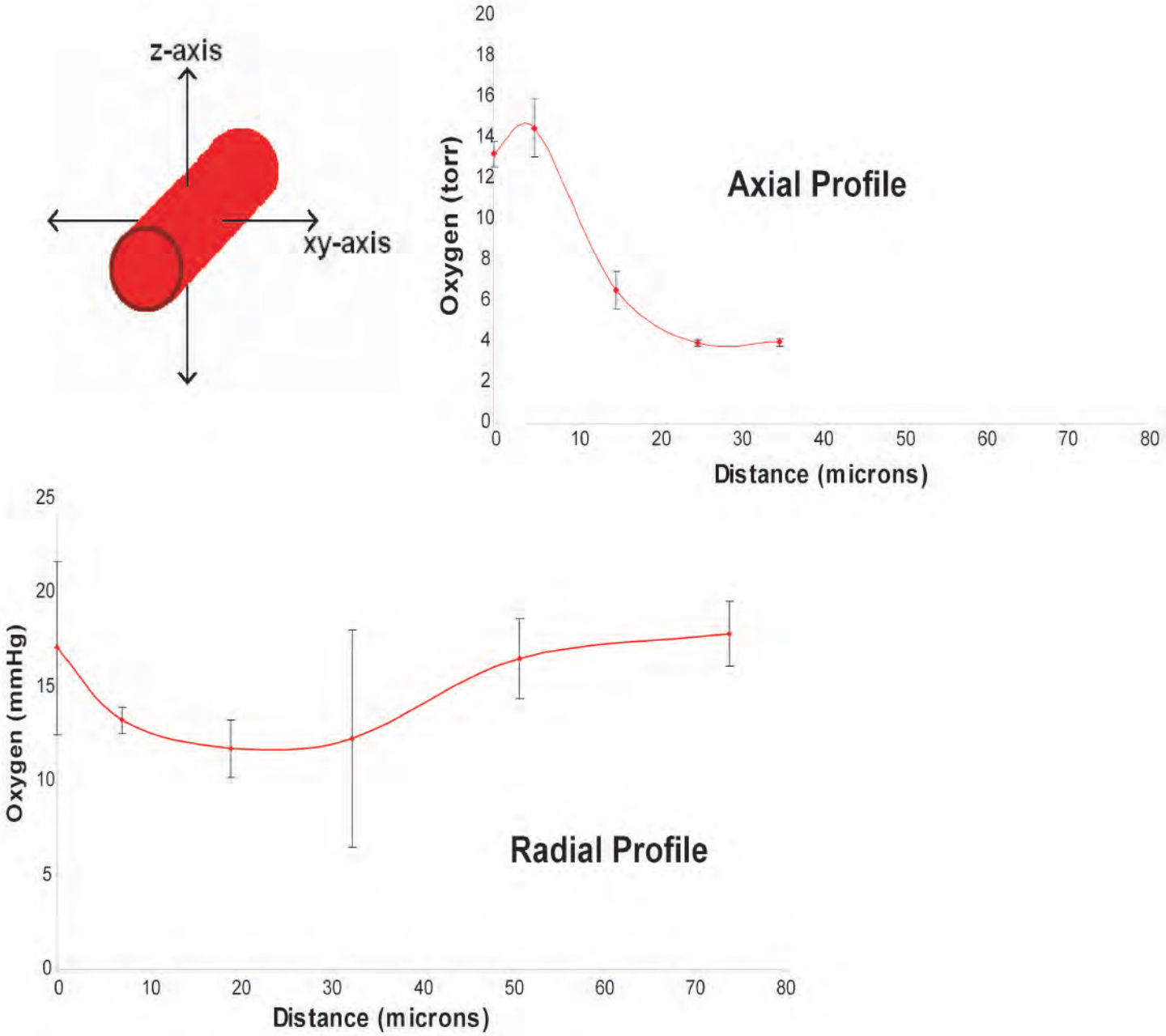

Figure 10: For a given tumor vessel, the radial and axial linear profiles can be very different suggesting a complex three-dimensional profile. The diagram in the upper left demonstrates the axes for the radial (xy) and axial (z) profiles.

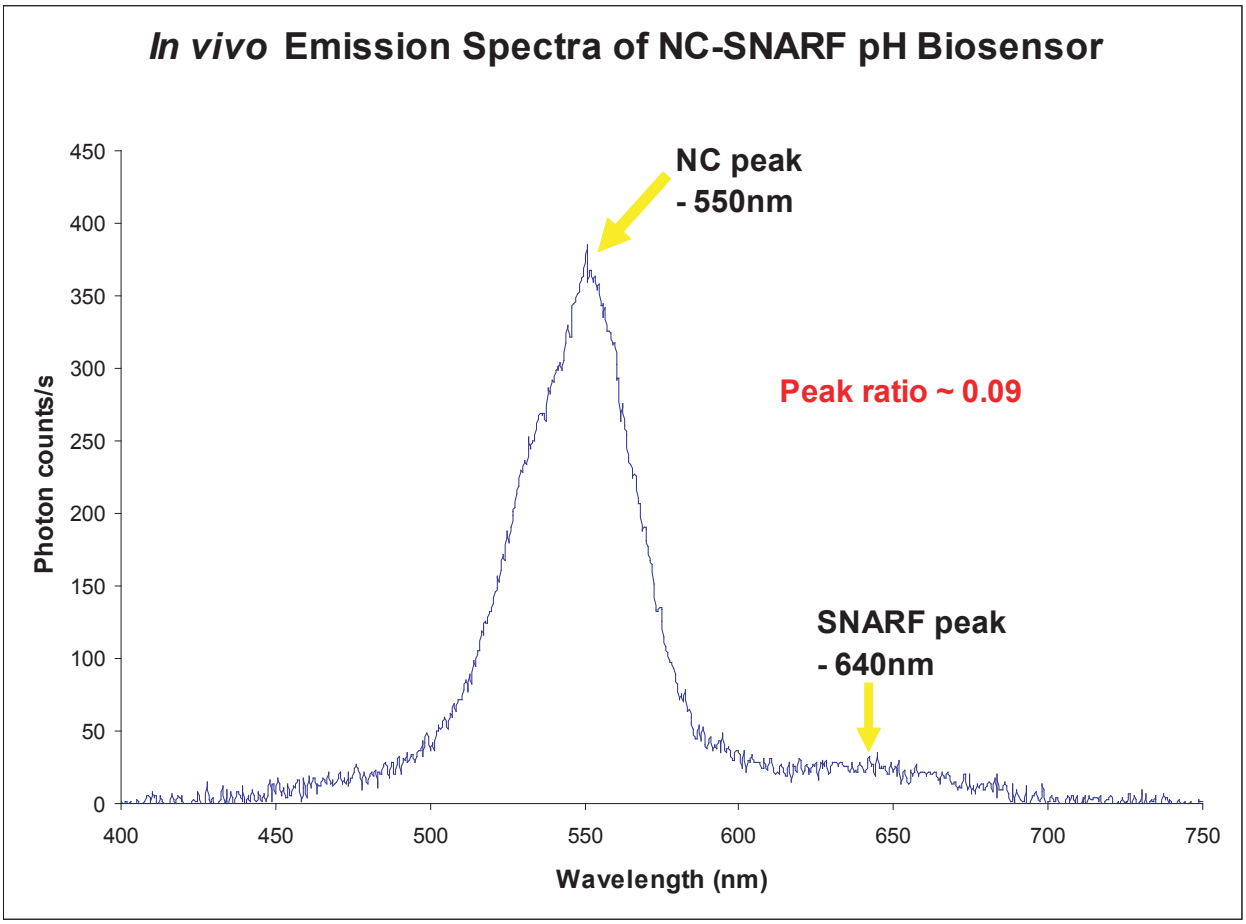

Figure 11: Emission spectrum of NC-biosensor obtained in vivo in a LLC1 tumor vessel. The NC peak is far larger than the pH-sensitive dye peak making analysis by imaging difficult. The ratio of the SNARF to the NC peak gives a value of 0.09, which according to figure 5 is a pH of ~ 7.

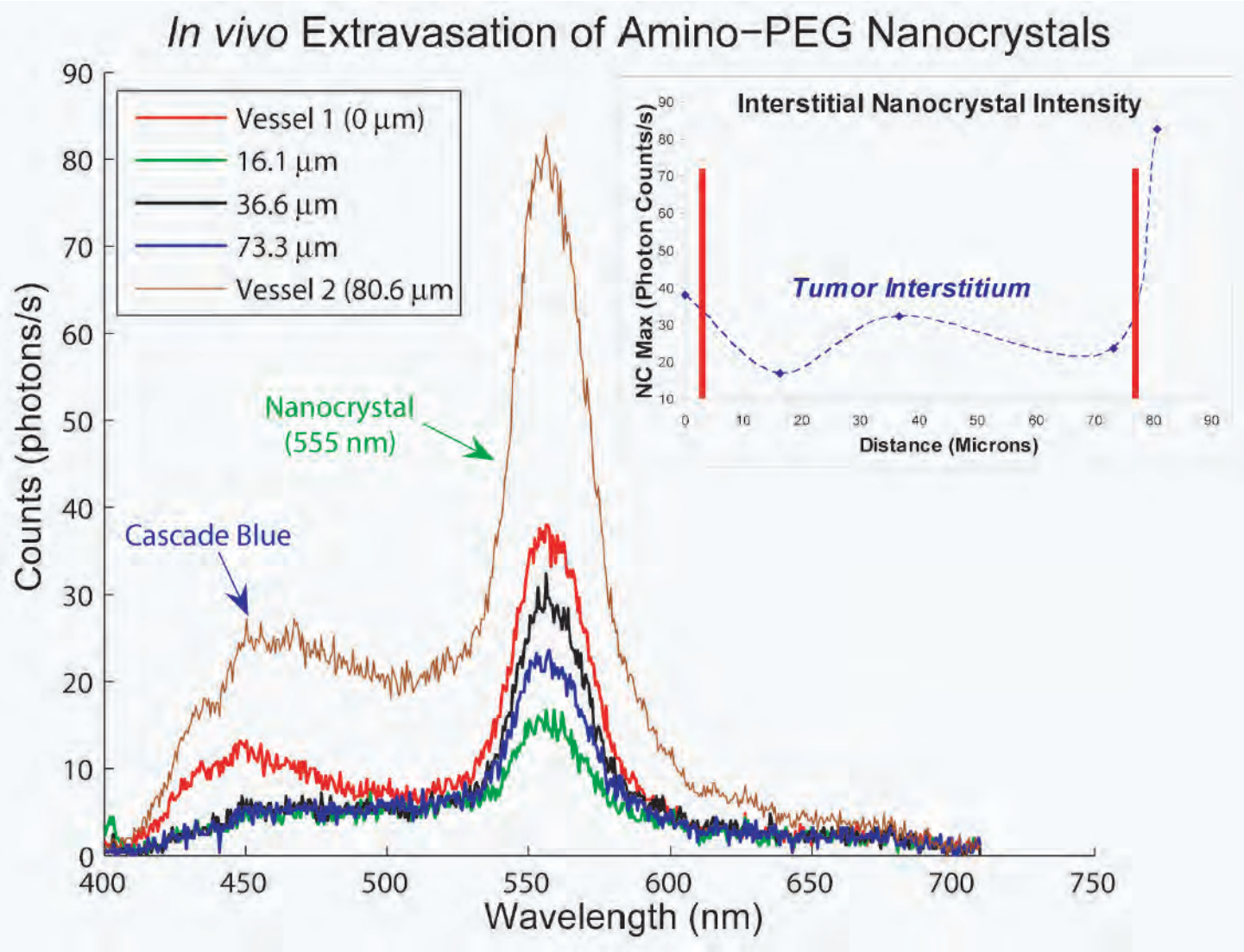

Figure 12: Intravenously injected amino-PEGylated nanocrystals demonstrate extravasation from the tumor vasculature of an MCaIV tumor grown in the MFP chamber less than 30 minutes post-injection with excitation by MPLSM. When a tumor vessel is imaged, emission spectra show both cascade blue bound to 500k MW dextran (~450nm, vascular imaging agent) and NCs (~555nm). Only the NC emission is present in the interstitial space of the tumor (black, blue and green). The upper graph plots the peak NC emission versus distance between two tumor vessels (red lines) in the focal plane of the MSPLM at 150 µm depth in the tumor.

J|A|C|S
COMMUNICATIONS

Published on Web 09/26/2006

A Ratiometric CdSe/ZnS Nanocrystal pH Sensor

Preston T. Snee,† Rebecca C. Somers, Gautham Nair, John P. Zimmer, Moungi G. Bawendi,* and Daniel G. Nocera*

Department of Chemistry, Massachusetts Institute of Technology, 77 Massachusetts Avenue, Cambridge, Massachusetts 02139-4306

Received March 20, 2006; E-mail: mgb@mit.edu; nocera@mit.edu

Semiconductor nanocrystals (NCs) serve as useful fluorescent labels owing to their photostability, continuous absorption spectra, and efficient, narrow, and tunable emission.[1−3] These properties of NCs have been exploited for applications in biological imaging[4] and in single particle tracking studies.[5] Whereas NCs are useful in identifying position in a microenvironment, their intrinsic insensitivity to the presence of most biological or chemical agents renders them of limited utility as sensing probes of that microenvironment. An important step in this direction has been the recent development of water-soluble CdSe NCs with the ability to sense target analytes irreversibly using fluorescence resonant energy transfer (FRET) as a signal transduction mechanism.[6−8] These previous studies, however, do not demonstrate reversible and ratiometric chemical sensing using fluorescent NCs. We now show that a reversible NC-based fluorescent sensor can be designed by conjugating a dye with an equilibrium response to an analyte to the surface of a CdSe/ZnS NC. We show that properly controlling energy transfer between the NC and dye engenders a general method for the development of ratiometric NC sensors, thus providing a means for detecting analytes with high precision, irrespective of changes in excitation intensity, wavelength, or collection efficiency. Our constructs thus remove several difficulties encountered with dye-only-based ratiometric nanoscopic sensing systems.[9]

High quality CdSe NCs overcoated with ZnS and capped with trioctylphosphine oxide ligands[10,11] were encapsulated by a hydrophobically modified poly(acrylic acid) (Figure 1).[12] The squaraine

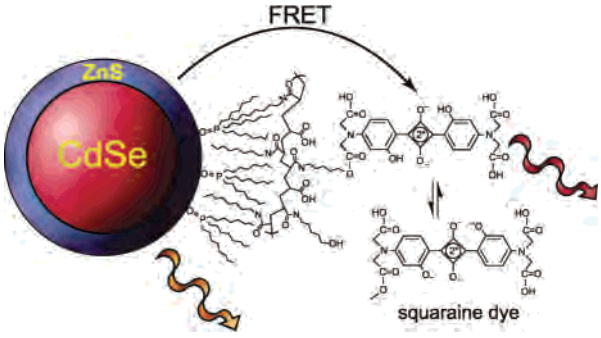

Figure 1. A sensor constructed from a colloidal CdSe NC that is overcoated with an outer layer of ZnS. The native phosphine oxide ligands are encapsulated with an amphiphilic polymer upon which a pH-sensitive squaraine dye is conjugated. Upon excitation, the CdSe/ZnS nanocrystal may either fluoresce or transfer energy to the squaraine dye. The FRET efficiency is modulated by the environment as the dye's absorption profile is a function of pH. Consequently, the ratio of NC to dye emission becomes a function of environmental variables.

dye[13] shown in Figure 1 was linked to the polymer backbone via ester linkages using 1-ethyl-3-(3-dimethylaminopropyl)carbodiimide (EDC) as the coupling agent. We have also found that the same dye conjugation method may be applied to water-soluble NCs that have been cap exchanged with thiol-functionalized poly(ethylene glycol)s.[14] The samples can be easily purified with dialysis filters to ensure that unreacted dyes are removed from the sample. The complete procedures for the synthesis of CdSe/ZnS NCs and squaraine dye and their subsequent conjugation are given in the Supporting Information (SI).

The sensing action of the NC−squaraine conjugate is imparted by modulation of the FRET efficiency arising from the engineered overlap of the pH-sensitive dye absorption spectrum with the (pH-insensitive) quantum dot emission (Figure S1 of SI). Owing to the pH dependence of the dye absorption spectrum, the spectral overlap between the dye absorption and the NC emission increases as the pH is lowered. This spectral overlap integral J is directly related to the critical FRET distance, R_o, which in turn affects the energy transfer efficiency $E(R_o)$ as shown in eq 1:

$$J(\mathrm{pH}) = \int \mathrm{d}\lambda \epsilon_{\mathrm{pH}}(\lambda)\mathrm{d}(\lambda)\lambda^4,\ R_o \propto J^{1/6},\ E(R_o) = \frac{R_o^{\,6}}{R_o^{\,6} + R^6} \quad (1)$$

where λ is wavelength, $\epsilon_{\mathrm{pH}}(\lambda)$ is the pH-dependent molar absorptivity, $\mathrm{d}(\lambda)$ is the normalized NC donor emission, and R is the donor−acceptor distance. The inset of Figure S1 shows a calculation of R_o as a function of pH; details of the FRET calculation are included in the SI. At high pH, FRET should be inefficient as the spectral overlap is small. Hence, the emission spectrum should be dominated by luminescence from the NC. As the pH is lowered, R_o grows larger and the FRET efficiency increases owing to a strengthening of the dye absorption cross section $\epsilon_{\mathrm{pH}}(\lambda)$. The NC emission should then be quenched as a result of energy transfer to the dye, which will in turn become more emissive.

The experimental results shown in Figure 2 are consistent with the calculated trend in R_o and expected FRET efficiency. The inset shows the response of the absorption profile of the NC−dye conjugate above and below the pK_a (∼8.5) of the dye. As observed for the free dye in homogeneous solution (Figure S1), the dye absorption band is suppressed under basic conditions. Consequently, energy transfer from the NC to the dye is inefficient, and the emission spectrum is dominated by the NC at 613 nm. As pH is lowered, the absorption cross section of the dye is increased, and FRET from the NC to the dye becomes more efficient; emission from the NC−dye conjugate is now dominated by that of the dye at 650 nm. The largest changes occur near the pK_a of the dye. The steady-state emission results are confirmed by time-resolved emission studies of the NC−dye conjugate. As shown in Figure S3, NC emission of a conjugated sensor has a reduced lifetime as compared to that of the unconjugated NC. These results establish that the emission from the NC donor is quenched by the presence of the organic dye acceptor, as has been previously observed in other constructs.[6,7]

† Present address: Department of Chemistry, The University of Illinois at Chicago, Chicago, IL 60607.

10.1021/ja0618999 CCC: $33.50

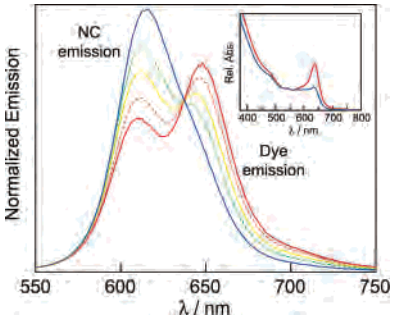

Figure 2. The emission profile of a water-soluble (3.2 nm radius) NC−squaraine dye conjugate changes as a function of pH (red solid line, 6.0; orange dotted line, 7.0; yellow solid line, 8.0; green dotted line, 9.0; and blue solid line, 10) with $\lambda_{ex} = 380$ nm. The normalized spectra show pH dependence with an isosbestic point appearing at 640 nm. The absorbance of the squaraine dye is suppressed in the conjugate at basic pHs as shown in the inset. The overall quantum yield of this construct is 7 ± 1%. Deconvolution of the absorption spectra into dye and NC components reveals that the dye to NC ratio is (3.4 ± 0.2):1. Shown in Figure S2 of the SI are the data from a 7.5:1 dye to NC conjugated sensor.

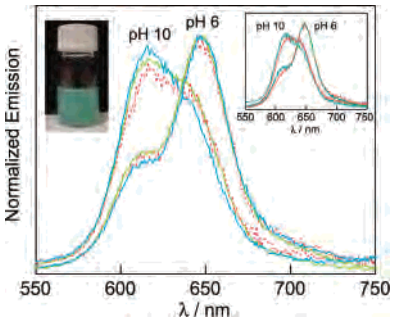

Figure 3. Sensing of the local pH by the NC/dye construct with variations in the excitation intensity and local environment. The ratio of NC to dye emission varies such that pH is determined within 5% when altering the slit entrance of the Xe lamp excitation of the fluorimeter (red dotted line, 0.5 mm; green solid line, 2.00 mm) and when examining the construct within a highly scattering media (blue solid line) shown by the picture of the vial. The inset shows that emission was independent of excitation wavelength (blue solid line, 380 nm; green solid line, 450 nm; red solid line, 520 nm).

The modulation of the FRET efficiency by pH results in an emission dependence between the NC and dye that is naturally ratiometric. Notably, the change in the NC−dye emission occurs about an isosbestic point at 640 nm. The solution pH can be read out precisely by taking the ratio of each emission peak intensity (NC and dye) to the intensity at the isosbestic point, which functions as an internal reference (or by measuring the ratio of any two unique points). This ratiometric approach is powerful when compared to typical chemo- and biosensors that display a single intensity-based response to analytes (i.e., either brightening or darkening) because the ratiometric construct is not sensitive to fluctuations of light excitation or collection efficiency as sensing is self-referencing.[15,16]

To highlight the importance of the self-referencing capability of our constructs compared to other organic sensing nanomaterials, we have examined the results of modulating the excitation intensity and wavelength on the normalized fluorescent spectra of the sensor in pH 6 and pH 10 buffered solutions. In separate experiments, ~130 nm silica microspheres were added to the solutions to produce a highly scattering medium. The results are shown in Figure 3. Using the ratio of NC to dye emission in clear solutions as a calibration, we are able to determine the pH within 5% when altering the excitation intensity over ~1 decade and varying the composition of the environment. Such precision is impossible to achieve for the dye alone. In addition, the continuous absorption manifold of the CdSe NCs results in a excitation-wavelength-independent band shape (see inset, Figure 3), a feature that is not present in single molecular ratiometric sensors.[17] Thus, the NC−dye conjugate does not need to use two independent excitation sources (or alternatively a single excitation specifically at an absorptive isosbestic point) for proper function.

In summary, we have developed a new strategy for chemical and biological sensing by tethering emissive water solubilized NCs to environmentally sensitive dye molecules. We have observed a ratiometric response to pH owing to modulation of FRET efficiency between the emissive NC and dyes conjugated to the NC surface. The approach is general as a sensing construct because the narrow, size-tunable emission spectrum of NCs enables them to be FRET donors that may be easily custom-engineered to match the acceptor absorption features of a dye conjugated to the surface of the NC. Taken together with the broad excitation spectrum and photostability conferred by NCs, the reversible and ratiometric approach presented here makes NCs versatile agents for chemical and biological sensing.

Acknowledgment. The authors would like to thank Y. Chan for helpful discussions. This work made use of the MRSEC Shared Facilities supported by the NSF under Award Number DMR-0213282, as well as the Harrison Spectroscopy Laboratory (NSF-011370-CHE). M.G.B. and D.G.N. acknowledge support from a Collaborative Research in Chemistry Grant by the NSF (NSF-CHE-020989). M.G.B. also acknowledges support from the NIH funded MIT−Harvard NanoMedical Consortium (1U54-CA119349, a Center of Cancer Nanotechnology Excellence), and the ARO through the Institute for Collaborative Biotechnologies. D.G.N. acknowledges support from Corning Inc.

Supporting Information Available: Full synthetic procedures and NMR spectra for the preparation of pH-sensitive squaraine dyes, water solubilized core shell NCs, and the conjugation of the two. Time-resolved emission of NC versus NC/squaraine dye conjugates as well as results from other pH-sensing conjugates. This material is available free of charge via the Internet at http://pubs.acs.org.

References

(1) Dahan, M.; Levi, S.; Luccardini, C.; Rostaing, P.; Riveau, B.; Triller, A. *Science* **2003**, *302*, 442.
(2) Michalet, X.; Pinaud, F. F.; Bentolila, L. A.; Tsay, J. M.; Doose, S.; Li, J. J.; Sundaresan, G.; Wu, A. M.; Gambhir, S. S.; Weiss, S. *Science* **2005**, *307*, 538.
(3) Lidke, D. S.; Nagy, P.; Heintzmann, R. Arndt-Jovin, D. J.; Post, J. N.; Grecco, H. E.; Jares-Erijman, E. A.; Jovin, T. M. *Nat. Biotechnol.* **2004**, *22*, 198.
(4) Alivisatos, A. P. *Nat. Biotechnol.* **2004**, *22*, 47.
(5) Pouya, S.; Koochesfahani, M.; Snee, P. T.; Bawendi, M. G.; Nocera, D. G. *Exp. Fluids* **2005**, *39*, 784.
(6) Goldman, E. R.; Medintz, I. L.; Whitley, J. L.; Hayhurst, A.; Clapp, A. R.; Uyeda, H. T.; Deschamps, J. R.; Lassman, M. E.; Mattoussi, H. *J. Am. Chem. Soc.* **2005**, *127*, 6744.
(7) Clapp, A. R.; Medintz, I. L.; Mauro, J. M.; Fisher, B. R.; Bawendi, M. G.; Mattoussi, H. *J. Am. Chem. Soc.* **2004**, *126*, 301.
(8) Medintz, L.; Konnert, J. H.; Clapp, A. R.; Stanish, I.; Twigg, M. E.; Mattoussi, H.; Mauro, J. M.; Deschamps, J. R. *Proc. Natl. Acad. Sci. U.S.A.* **2004**, *101*, 9612.
(9) Sumner, J. P.; Aylott, J. W.; Monson, E.; Kopelman, R. *Analyst* **2002**, *127*, 11.
(10) Murray, C.; Norris, D. J.; Bawendi, M. G. *J. Am. Chem. Soc.* **1993**, *115*, 8706.
(11) Dabbousi, B. O.; Rodriguez-Viejo, J.; Mikulec, F. V.; Heine, J. R.; Mattoussi, H.; Ober, R.; Jensen, K. F.; Bawendi, M. G. *J. Phys. Chem. B* **1997**, *101*, 9463.
(12) Wu, X.; Liu, H.; Liu, J.; Haley, K. N.; Treadway, J. A.; Larson, J. P.; Ge, N.; Peale, F.; Bruchez, M. P. *Nat. Biotechnol.* **2003**, *21*, 41.
(13) Isgor, Y. G.; Akkaya, E. U. *Tetrahedron Lett.* **1997**, *38*, 7417.
(14) Uyeda, H. T.; Medintz, I. L.; Jaiswal, J. K.; Simon, S. M.; Mattoussi, H. *J. Am. Chem. Soc.* **2005**, *127*, 3870.
(15) Liu, J.; Diwu, Z.; Leung, W. Y. *Bioorg. Med. Chem. Lett.* **2001**, *11*, 2903.
(16) Rink, T. J.; Tsien, R. Y.; Pozzan, T. *J. Cell. Biol.* **1982**, *95*, 189.
(17) Grynkiewicz, G.; Poenie, M.; Tsien, R. Y. *J. Biol. Chem.* **1985**, *260*, 3440.

JA0618999

CdSe nanocrystal based chem-/bio- sensors

Rebecca C. Somers, Moungi G. Bawendi* and Daniel G. Nocera*

Received 11th September 2006
First published as an Advance Article on the web 27th February 2007
DOI: 10.1039/b517613c

Semiconductor nanocrystals (NCs) have found application in biology mostly as optical imaging agents where the photophysical properties of the NCs are insensitive to species in their environment. This *tutorial review* examines the application of CdSe NCs as optical sensing agents where the NC's photophysical properties are sensitive to species in their environment. For this case, the NC is modified at the surface with a conjugate, which interacts with an external agent by physical (*i.e.* recognition) or chemical means. Signal transduction in these chem-bio (CB) sensitive NCs is derived primarily from energy transfer between the NC and the external agent, which functions as the energy transfer acceptor or donor. Signaling may be obtained by directly detecting luminescence from the NC and/or the conjugate. New developments for the use of NCs as gain materials in micro-lasing cavities (distributed feedback gratings and spherical resonators) opens the way to designing CB-sensitive NCs for high-gain sensing applications.

Department of Chemistry, Massachusetts Institute of Technology, 77 Massachusetts Avenue, Cambridge, MA, 02139-4307, USA

Rebecca C. Somers

Rebecca C. Somers received her BA in Chemistry from Northwestern University in 2003. Currently she is in her fourth year of graduate studies at MIT, working in the laboratories of Prof. Daniel G. Nocera. She is on a collaborative project between Profs. Nocera and Bawendi, studying the application of quantum dots for sensing.

Semiconductor nanocrystals as fluorophores and imaging agents

Inorganic semiconductor nanocrystals (NCs, also known as quantum dots) are a class of fluorophores that have attracted considerable interest owing to their unique photophysical characteristics. The electronic properties of NCs are determined by the physical confinement of excitons, which are excited electrons bound through Coulombic interactions to the holes left behind in the valence band. Quantum confinement in semiconductors occurs when the dimensions of the NC approaches that of the exciton. The effective bandgap of the NC widens with decreasing size, giving rise to unique, size-dependent optical and spectroscopic properties.[1] Broad absorption profiles and high extinction coefficients are complemented by a narrow (full-width-half-maximum $\sim$30 nm) and spectrally tunable emission profile. Fig. 1 shows the size-dependent optical properties of CdSe nanocrystals. For

Moungi G. Bawendi

Prof. Moungi G. Bawendi received his AB in 1982 from Harvard University and his PhD in chemistry in 1988 from The University of Chicago. Following two years of post-doctoral research at Bell Laboratories with Dr Louis Brus, Bawendi joined the faculty at MIT in 1990, becoming Associate Professor in 1995 and Professor in 1996. He has followed an interdisciplinary research program that aims at probing the science and technology of chemically synthesized nanocrystals of semiconductor materials. Since beginning his independent career at MIT, he has been recognized for his pioneering contributions to the fundamental science of semiconductor nanocrystals, as well as for their applications in opto-electronics and in biological imaging.

Daniel G. Nocera

Daniel G. Nocera is the W. M. Keck Professor of Energy at the Massachusetts Institute of Technology. He received his BS degree from Rutgers University in 1979 and his PhD degree from Caltech in 1984. He has studied the mechanisms of biological and chemical energy conversion, contributing heavily to the basic science needed for developing solar-based renewable energy. These studies have led to his interest in the control of excited state processes for a variety of applications including optical sensing.

Fig. 1 Size-dependent emission properties of highly luminescent CdSe/ZnS NCs. From left to right, solution emission maximums are at 470, 480, 520, 560, 594, and 620 nm. Photograph by Felice Frankel. Quartz cuvettes courtesy of Spectrocell Inc. (Reproduced with permission from *J. Phys. Chem. B*, 1997, **101**, 9463.[3] Copyright 1997 American Chemical Society.)

example, small (2.3 nm diameter) CdSe NCs emit blue light under optical excitation whereas their larger counterparts (5.5 nm diameter) emit red light. The NCs exhibit appreciable quantum efficiencies for emission, though coating the outer surface of NCs with higher band gap inorganic materials further improves the photoluminescence quantum yield. The coating presumably passivates sites associated with surface states that promote nonradiative recombination.[2,3] Along with higher quantum yields, ''overcoated'' core/shell CdSe/ZnS NCs are more robust and possess high photobleaching thresholds.[1] These properties of NCs contrast with organic dyes, which tend to possess low resistance to photobleaching, narrow absorption profiles, and emission spectra that tail to the red; the spectral congestion that results from the tailing emission profiles can complicate multi-color imaging applications.[4]

Despite the apparent advantages of NCs as compared to organic dyes, the implementation of NCs for fluorescence imaging was initially hampered by their insolubility in aqueous media as a result of the long-chained organic solvents needed for their high-temperature synthesis. This obstacle was overcome by further modifying the surface of the CdSe NCs.[3] Alivisatos and co-workers prepared bio-compatible CdSe/CdS or CdSe/ZnS NCs by adding a third layer of silica to the core/shell.[5] Nie and co-workers reported the use of mercaptoacetic acid to cap the surface of CdSe/ZnS NCs to impart water-solubility.[6] The synthesis of water-soluble NCs now includes modifications with phospholipids,[7] amphiphilic polymers,[8] dendrimers,[9] oligomeric phosphines[10] and cap-exchanging the hydrophobic surface of NCs with multidentate hydrophilic ligands.[11] These ligands have greatly facilitated the use of NCs as bio-imaging agents and probes because they can be conjugated to proteins and peptides, such as streptavidin for cell-labeling studies.[4] The stability and quantum yields of such water-soluble NCs greatly vary among the different solubilization methods. For example, mono-thiol caps are photochemically unstable,[12] whereas multidentate ligands are reported to yield an aggregate-free construct and to be stable in solutions of pH 5–12 over a course of one year with quantum yields around 25–30%.[11] Toxicity of NCs is a concern for biological *in vivo* experiments; however, most studies report no toxicity in live animals, even in embryos under standard conditions.[4] Oxidation of CdSe by air or UV light can cause Cd^{2+} to be released, which is toxic to cells.[13] Protection of NCs from oxidation reduces toxicity, but long term cadmium leaching from NCs has not been studied.

More recently, the utility of NCs has been expanded by their use as optical sensors.[14] Initial applications centered on physical sensing. Walker *et al.* used the temperature-dependent photoluminescence properties of CdSe/ZnS nanocrystals embedded in poly(lauryl methacrylate) to develop a temperature probe.[15] These initial studies have subsequently been elaborated for the measurement of temperature[16] and fluid flow near walls and in confined channels[17] opening the way for tandem flow measurements of temperature and velocimetry.

The water-solubility of overcoated NCs has rapidly led to their use as fluorescence chemical sensors. For this application, NC luminescence is perturbed by the presence of a target analyte in the NC's environment. In some cases, the fluorescence is suppressed by morphological changes to the lattice. For example, Ag^{+}, Pb^{2+}, and Cu^{2+} ions quench NC luminescence by replacing the Cd^{2+} ions in the nanocrystal lattice.[18] Only by overwhelming the NC with excess Cd^{2+} can luminescence be partially recovered. However, permanent quenching of NC luminescence is not practical as a sensing strategy, as it is usually not analyte specific, nor is it easily reversible. Recently, detection of specific chem-/bio- (CB) target analytes has been achieved reversibly using overcoated CdSe NCs that have been modified with a conjugate attached to the overcoated layer. We note that work has also been performed with NCs composed of materials other than CdSe, most notably CdTe.[19] However, the concepts of sensing and amplification strategies are most comprehensively embodied by CdSe. For this reason, CdSe NC constructs, together with the excited state mechanisms that underpin their sensing function, constitute the scope of this review.

Fluorescence energy transfer

Fluorescence resonance energy transfer (FRET) has been the primary photophysical mechanism by which NCs report the presence of a target analyte. FRET is a phenomenon in which photo-excitation energy is transferred from a donor fluorophore to an acceptor molecule. Förster theory correlates the rate for this energy transfer to the spectral overlap of donor emission and acceptor absorption and the donor–acceptor spatial arrangement.[20] The rate of energy transfer, $k_{D\rightarrow A,}$ is given by eqn (1) and (2),

$$k_{D\rightarrow A} = \frac{1}{\tau_D}\left(\frac{R_0}{r}\right)^6 \quad (1)$$

$$R_0 = \frac{9000\ \ln(10)\phi_D\kappa^2}{128\pi^5 n^4 N}\int_0^\infty dv \frac{f_D(v)\varepsilon_A(v)}{v^4} \quad (2)$$

where τ_D and ϕ_D are the lifetime and quantum yield of the donor, respectively, r is the distance between donor and acceptor, R_0 is the critical transfer distance, n is the refractive index of the medium, N is Avogadro's number, and κ^2 is a

constant reflecting the relative orientation of donor and acceptor dipoles. Although the NC is a fairly large object in proximity to the dye, NC-FRET studies make an approximation to treat the NC excited state as an oscillating point dipole and use $\kappa^2 = 2/3$ for a random orientation. Even with the point dipole approximation, many studies described below report that treating the NC based energy transfer through Förster theory described experimental data consistently. The overlap integral is comprised of $f_D(v)$, the normalized fluorescence intensity of the donor in wavenumbers (cm^{-1}), and $\varepsilon_A(v)$, the extinction coefficient of the acceptor. The R_0 is the distance where 50% of the excited donor will decay back to its ground state and the other 50% will transfer its energy to the acceptor molecule. As shown in eqn (2), the transfer distance is dependent mainly on the spectral overlap between the emission of the donor and the absorbance of the acceptor.

The efficiency (E) of FRET, or the fraction of photons absorbed by the donor that are transferred to the acceptor, is the ratio of the transfer rate to the total decay rate of the donor and is described by eqn (3):

$$E = 1 - \frac{\tau_{D-A}}{\tau_D} = \frac{k_{D-A}}{k_{D-A} + \tau_D^{-1}} = \frac{R_0^6}{R_0^6 + r^6} \quad (3)$$

Eqn (3) can be modified when more than one acceptor can interact equally with the donor as shown in eqn (4):

$$E = \frac{mR_0^6}{mR_0^6 + r^6} \quad (4)$$

Therefore, eqn (4) shows that the efficiency of energy transfer is generally enhanced by increasing the number of acceptor molecules, m. It is important to note in a study that utilizes one donor and multiple acceptors, any distance measurements derived will represent a statistical average distance in a given solution of donor–acceptor pairs unless every pair has an identical fixed distance between the donor and acceptor and an identical number of acceptors per donor.[21] As the energy transfer rate constant and corresponding efficiency depend on the inverse sixth power of intermolecular separation of donor and acceptor molecules, usually on lengths scales between 20 to 90 Å, the study of FRET is useful for distances comparable to biological macromolecules and is often applied for sensing changes in protein conformation and analyte binding events.[20] Investigations of FRET with NCs that have formed the underpinning for the use of NCs as chemical sensors are presented in the section below.

NC energy transfer

Energy transfer among CdSe NCs was observed by Kagan *et al.* when they prepared thin films comprised of a mixture of closely-packed smaller 555 nm emitting and larger 620 nm emitting NCs.[22] Steady-state emission from the smaller NCs decreased concomitantly with an increase in emission from the larger NCs. Correspondingly, the lifetime of the smaller NCs shortened while that of the larger NC lengthened. Analysis of the lifetime data by Förster theory supported the occurrence of energy transfer. This study established that CdSe NCs can act as both FRET donors and acceptors.

Energy transfer involving CdSe NCs in aqueous media has been observed to occur between oppositely charged CdSe/ZnS NCs. Wargnier *et al.* prepared negatively charged CdSe/ZnS by treating the NCs with a mixture of mercaptosuccinic and mercaptosulfonic acids.[23] Positively charged ZnCdSe–ZnS NCs were synthesized by treating the NC surface with cystinamine. Upon mixing with larger NCs (which naturally carry a negative charge), emission from the positively-charged and smaller NCs was found to be quenched. On the basis of the diameters of the NC donor and acceptors, a Förster critical distance and efficiency were calculated to be 7.3 nm and 91%, respectively; these values were in reasonable agreement to the Förster critical distance and efficiency determined from the quenching of the PL decay times.

NCs as FRET donors

Energy transfer from a NC donor to an organic acceptor in aqueous solution was demonstrated by Willard *et al.*[24] Water-soluble CdSe/ZnS NCs were conjugated to a thiolated biotinilated bovine serum albumin (bBSA, 9 : 1 biotin : BSA ratio). Calculations revealed that 11 bBSA molecules were bound to the surface of the NC. The acceptor complex was prepared separately by conjugating streptavidin to tetramethylrhodamine. Upon titrating the dye-modified streptavidin to the NC–bBSA complex in PBS buffer, NC luminescence was quenched and TMR fluorescence was enhanced.

A penetrating study of energy transfer between donor NCs and acceptor dye molecules has been performed by Mattoussi and co-workers.[21,25] Water-soluble CdSe/ZnS NCs were prepared by exchanging ligands on the NC surface with dihydrolipoic acid, which possesses bidentate thiol groups. A maltose binding protein (MBP) from an engineered *Escherichia coli* containing site-specific labeled dye acceptors was assembled onto the surface of the NC by either: (1) electrostatic self-assembly of the negatively charged dihydrolipoic acid to a basic leucine zipper on the MBP or (2) metal-affinity coordination between the NC surface and a C-terminal oligohistidine chain on the MBP (see Fig. 2).[21,25] In synthesizing these constructs, the emission wavelength of the NC and the number of dye-labeled MBPs bound to the NC were systematically varied. The total number of MBPs per NC was maintained for the different-sized NCs in order to maintain the average distance between the NC and the acceptor dyes and hence the same NC quantum yield. As the fraction of dye-labeled MBPs was increased, emission from the dye increased while that from the NCs decreased. Time-resolved fluorescence experiments confirmed that the NC lifetime shortened as more dye-labeled MBPs surrounded the NCs.[21,25] Additionally, experiments varying the spectral overlap (by changing the NC donor emission wavelengths) revealed that the efficiency of energy transfer varied as expected from a Förster model. As expected from eqn (4), efficiency improved with increasing numbers of dye-labeled MBPs around the NC.[21] All of these studies support an energy transfer mechanism between a CdSe NC donor and an organic acceptor dye.

Energy transfer between a NC donor and a dye acceptor has also been observed at the single molecule level.[26] Hohng *et al.* used a commercially available streptavidin-coated NC to

immobilize the NC on a quartz surface coated with bBSA. A cyanine dye, Cy5, was positioned near the NC surface by placing it with biotin on the same end of a duplex DNA. Energy transfer was monitored with the steady-state emission of the NC and Cy5. Observation of a single-molecule conformational change of the NC–Cy5 conjugate was also sought using a Holliday junction, which is composed of four DNA helices. The DNA junction changes its fold in the presence of divalent ions. Conformational change induced by the divalent ion would, in principle, lead to a change in FRET efficiency. However, very low signal intensity complicated such an interpretation. The low signal was ascribed, in part, to the very large energy transfer distance between the streptavidin-coated NC and biotinylated dye, emphasizing the need for simple conjugates in which the energy transfer distance can be short.

Zhou *et al.*[27] directly coupled an Alexa 594-labeled DNA acceptor to a NC donor through a thiol linker. Commercially obtained CdSe/ZnS NCs were treated with 3-mercaptopropionic acid (MPA) to produce a water-soluble NC. Coupling to Alexa 594-labeled DNA was achieved using a C_6 thiol linker. The ability to couple without protein linkers minimized the distance between the NC and the dye. Owing to the short donor–acceptor distance, the FRET efficiency in these constructs was found to be as high as 88% in ensemble and single-molecule constructs. A Förster critical transfer distance of 4.2 nm was calculated from the quenched luminescence.

NCs as FRET acceptors

Whereas there have been numerous studies on CdSe NCs as FRET donors, very few studies have reported CdSe NCs as FRET acceptors. Mattoussi and co-workers investigated the potential of CdSe NCs as energy acceptors from organic donor dyes by using a NC–dye MBP conjugate in which the dye emitted to the blue edge of the NCs.[28] AlexaFluor 488 and Cy3 dyes were employed to excite NCs of three different sizes. No evidence of energy transfer from the dye to the NC was found in steady-state and time-resolved emission experiments for dye : NC ratios up to 1 : 10. Tryptophan residues in the MBP were also excited to see whether FRET could occur between the amino acid and the NC. But again, there was no evidence of tryptophan quenching. Energy transfer from an organic dye to a CdSe NC is difficult to achieve for two reasons. First, the radiative decay rate of the dye donor excitation energy is fast compared to the decay rate for FRET from dye to the NC acceptor. In addition, the NC could be directly excited, which

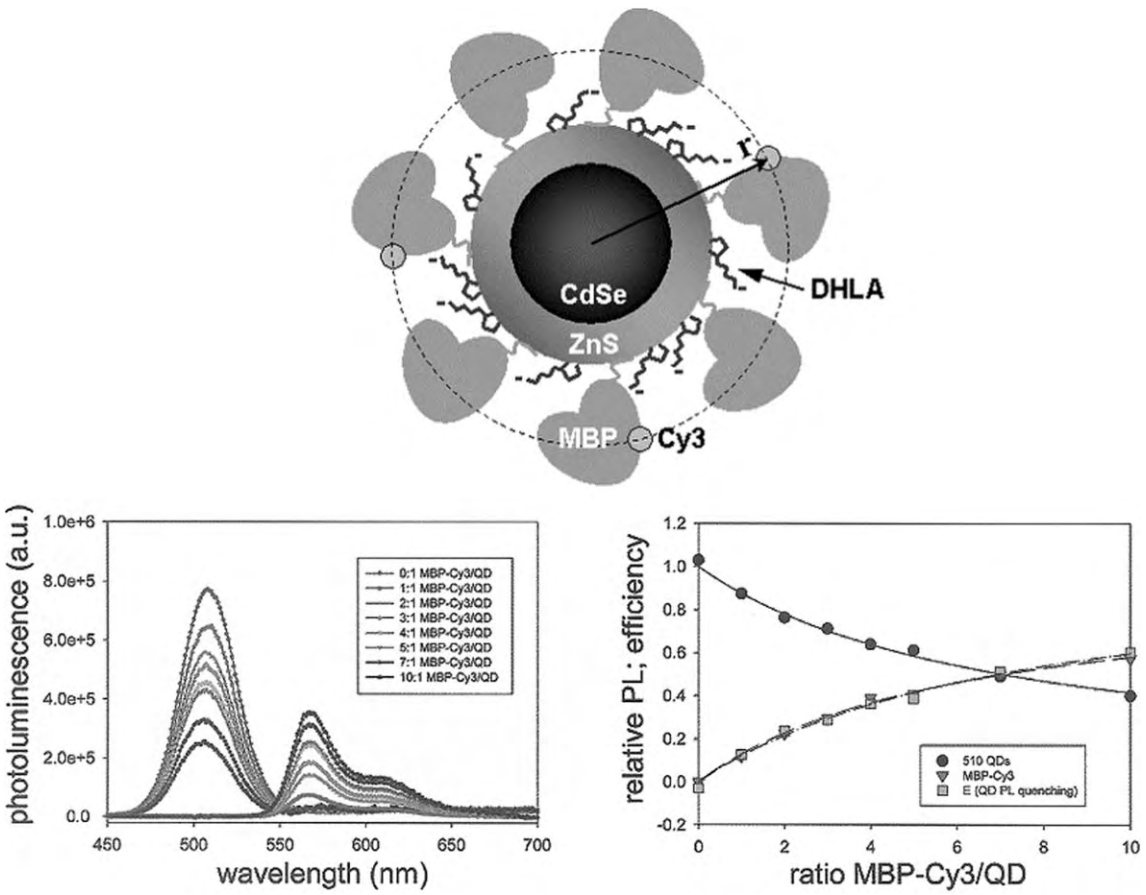

Fig. 2 (Top) A schematic representation of the NC-MBP assembly developed by Mattoussi and co-workers. The dihydrolipoic acid (DHLA) caps the NC and allows the MBP to self-assemble onto the NC. A Cy3 dye is attached to the MBP. (Bottom left) Photoluminescence spectra from 510 nm emitting NC and Cy3 dyes in the NC–MBP–Cy3 construct with increasing dye to NC ratio. (Bottom right) Experimental values for the NC emission decay percentage *versus* dye to NC ratio (circle), the rate of FRET extracted for the NC emission loss (triangle), and the rate of FRET deduced from acceptor gain (square). (Reproduced with permission from *J. Am. Chem. Soc.*, 2004, **126**, 301.[21] Copyright 2004 American Chemical Society.)

causes difficulties in ascertaining the FRET contribution to the observed NC emission. In order to test whether the lifetime of the donor was limiting FRET, a dye with a longer-lived excited state (a ruthenium–bpy–isothiocyanate complex with τ_o = 350 ns) was covalently appended to the MBP. Steady-state fluorescence experiments, however, were inconclusive owing to a high degree of emission spectral overlap between the ruthenium complex and the NC together with the low quantum yield of the complex. Time resolved measurements, however, did reveal quenching of the dye excitation lifetime, implying the occurrence of FRET.

Further support for the use of CdSe as energy acceptors has been provided by Acherman *et al.*, who have reported energy transfer between InGaN quantum wells and CdSe NCs.[29] A three-layer heterostructure was made by depositing a layer of CdSe NC through the Langmuir–Blodgett technique onto a GaN-capped InGaN quantum well. In this case, energy transfer rate of carrier varied as $1/d^4$, where d was the separation distance between the quantum well donor and the NC acceptor. The efficiency of energy transfer was found to be as high as 55%.

Blue-emitting polymers may act as FRET donors to NCs at 18 K.[30] Energy transfer from a conjugated organic polymer, {poly[(9,9-dihexylfluorenyl-2,7-diyl)-alt-co-(9,ethyl-3,6-carbazole)]} to CdSe/ZnS NCs was confirmed by the quenching of the polymer lifetime and by the appearance of NC emission upon excitation of the polymer. The calculated Förster radius of 8 nm (though this value is somewhat tenuous since it could not be corrected for direct excitation of the NCs) is comparable to that of organic FRET donor–acceptor pairs.

Commercially biotinylated NCs and streptavidin can be conjugated to a terbium ion ligated by two 6-carboxybipyridyl arms connected to a glutamate framework.[31] Carbodiimide coupling of the terbium complex yields an average of 3.5 terbium complexes per streptavidin protein. The NC was coated with 5 to 7 biotin molecules per NC. Upon titrating the biotinylated NC to the streptavidin–Tb complex, the lifetime of the NC is enhanced and the ratio of NC to Tb emission increased as well. These observations were attributed to the presence of FRET. An average donor–acceptor distance of 7.2–7.6 nm was determined for the FRET.

Anikeeva and co-workers have demonstrated energy transfer from a phosphorescent *fac* tris(2-phenylpyridine) iridium complex, $Ir(ppy)_3$, to a thin-film monolayer of CdSe/ZnS.[32] The $Ir(ppy)_3$ emission intensity decreased by 21% and the emission intensity of the CdSe/ZnS film increased by 55% when a monolayer of the NCs was printed on a film of 10% $Ir(ppy)_3$. A corresponding increase in the lifetime of the NC emission from 40 ns to 400 ns suggested the transfer of $Ir(ppy)_3$ excitons to the NC film. The distance between the iridium complex and the NC was estimated to be 4.0 nm, which is sufficiently short for Förster and Dexter (*i.e.*, correlated electron exchange) energy transfer to occur.

FRET schemes for sensing with NCs

The ability of NCs to participate in FRET provides a mechanism for signal transduction in optical sensing schemes. Fig. 3 summarizes the different sensing strategies that have been employed with NCs. Of the six signal transduction mechanisms, five rely on the NC as the FRET donor. The broad excitation spectrum of the NCs complicates their utilization as FRET acceptors since it is difficult to excite a dye selectively without exciting the NC acceptor. In Fig. 3A–3D, sensing is accomplished by modulating the FRET donor–acceptor distance. For Fig. 3E and 3F, the FRET distance is preserved but the analyte causes the spectral overlap function to change, thus modulating the efficiency of FRET upon analyte recognition. A discussion of systems that sense by each of the mechanisms presented in Fig. 3 follows.

3A: Sensing by nucleic acid recognition

Fig. 3A has been exploited to probe biological activity *via* FRET. Telomerization and DNA replication can be monitored with CdSe/ZnS NCs.[33] Patolsky *et al.* conjugated NCs to thiolated oligonucleotides with approximately 25 oligonucleotides per NC. Incubation with a dNTP (deoxy(nucleotide) triphosphate) mixture (dATP, dCTP, and dGTP) and Texas-Red labeled dUTP, in the presence of telomerase, initiated a change in the emission spectra of the NC and the dye over time. As telomerization proceeded, NC emission decreased and Texas-Red emission increased due to FRET. DNA replication was probed by labeling CdSe/ZnS NCs with a DNA primer, followed by incubation with the complementary DNA sequence to allow for hybridization. Replication was initiated by adding polymerase mixed with dNTPs and Texas-Red labeled dUTP. As replication progressed, the Texas-Red dUTP was brought in proximity to the NC, resulting in FRET from the NCs to the dye. These results suggested the application of NCs for the detection of cancer cells or for amplified detection of DNA on chip arrays.

Gill *et al.* have used FRET interactions of DNA to probe hybridization and cleavage.[34] In a similar manner to that discussed above, NCs were modified with a DNA strand and hybridized with a Texas-Red labeled nucleic acid. As hybridization proceeded, energy transfer occurred, and the NC emission progressively became weaker while the dye emission increased. The resulting CdSe NC–dye DNA duplex was cleaved with a hydrolytic enzyme DNase I. Cleavage of the DNA strand resulted in a partial restoration of the NC emission and a loss of dye emission. The incomplete recovery of the NC emission was attributed to the adsorption of dye molecules to the NC surface. Adsorption by the NCs presents a hurdle for their implementation as bioanalytical tools.

FRET from NCs can be used as a screen for small interfering RNAs (siRNA).[35] Bakalova *et al.* conjugated a single stranded siRNA to a NC to yield a hybridization probe while amplifying the target mRNA in the presence of Cy5 labeled nucleotides. The Cy5–mRNA was used as the hybridization template. A short hybridization time for siRNA–mRNA duplexes ensured for the selection of efficient, target-selective siRNA sequences. The affinity of the siRNA to the mRNA was detected by FRET from the NC to the Cy5. The Cy5 emission was only detected when there was good accessibility and high affinity between the two RNA strands.

The interaction of a HIV-1 regulatory protein, REV with its responsive element (designated RRE), has also been

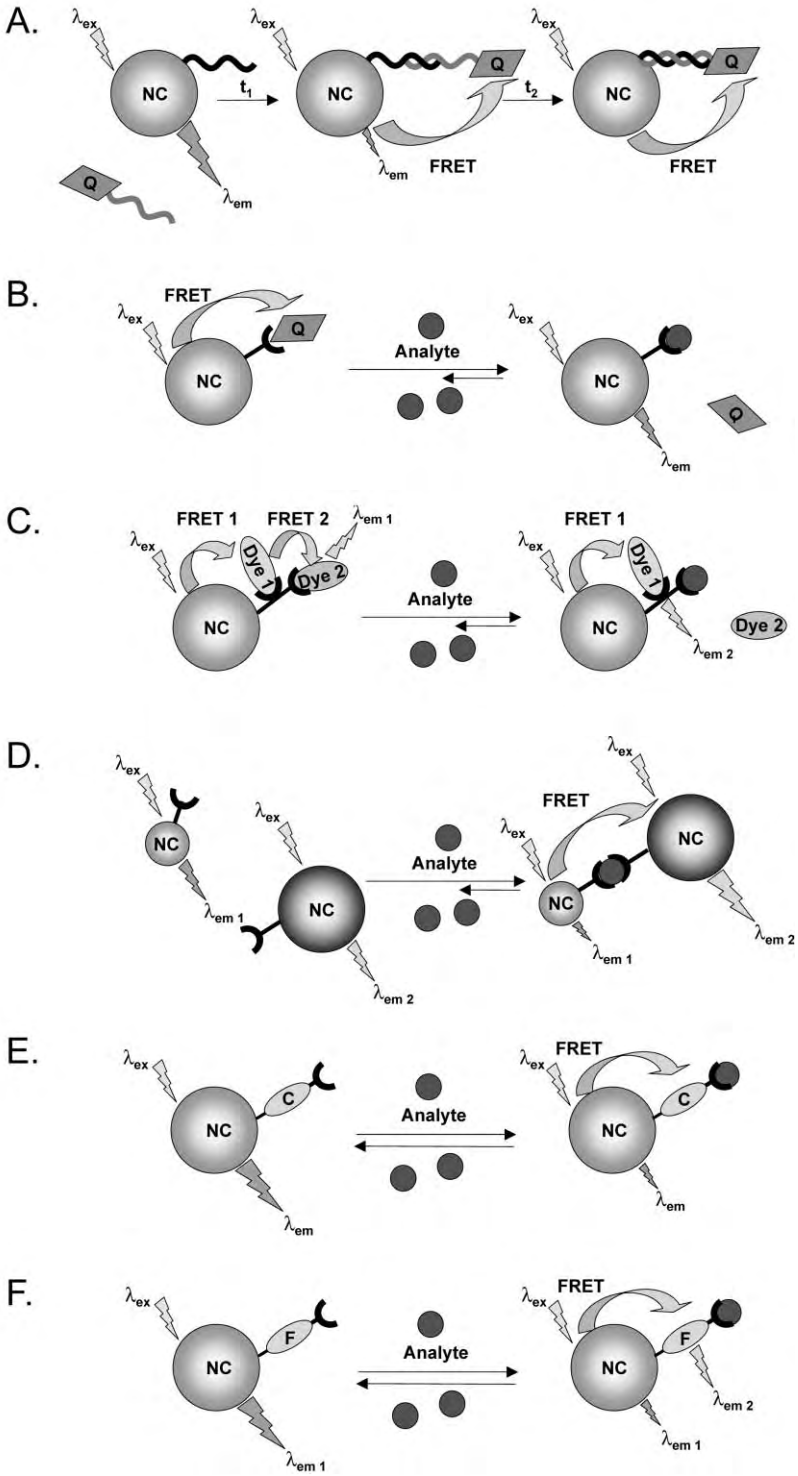

Fig. 3 Schematic diagram of the six different sensing strategies using FRET that are the focus of this tutorial review.

assayed by NC–dye FRET.[36] The 5′ end of the RRE RNA was biotinylated while a Cy5 dye was attached to the N-terminus of a model REV peptide sequence. A RRE–NC conjugate was synthesized by using a streptavidin-coated NC. The Cy5 modified REV was slowly titrated to the RRE–NC solution. Excitation at 488 nm, where the Cy5 does not absorb, yielded emission from both NC and Cy5 upon complexation of the REV to the RRE–NC. The ratio of the dye intensity to NC intensity increased with the addition of REV.

Per Fig. 3A, the foregoing bioassays rely on modulating the FRET distance between the NC and an acceptor dye upon biological recognition of different macromolecules. A change in emission lifetime and intensity may be detected. Applications based on this model assume that the NCs do not interfere with macromolecule binding as a result of either

size or charge perturbations. This assumption must be assessed for the development of reliable bioassays.

3B and 3C: Sensing by analyte-induced displacement

FRET coupled to quenching, as schematically represented in Fig. 3B and 3C, provides alternative strategies for sensing. Here, luminescence due to FRET is turned on by the appearance of analyte, which displaces a quencher (Fig. 3B) or a terminal energy acceptor (Fig. 3C).

Mattoussi and co-workers have developed a sensor for maltose by adapting their CdSe–MBP conjugates for both analyte-displacement strategies depicted by Fig. 3B and 3C.[37,38] In the first construct, a β-cyclodextrin (β-CD) conjugated to a non-fluorescent QSY9 quencher dye was docked to the MBP saccharide binding site of the CdSe/ZnS–MBP. Maltose displaces the β-CD–QSY9 conjugate to restore NC emission. In their second strategy, defined by Fig. 3C, the CdSe/ZnS–MBP construct is labeled with two different cyanine dyes: Cy3, which is bound directly to the MBP, and a β-CD conjugated to a Cy3.5, docked to the MBP binding site. Prior to maltose binding, Cy3.5 emission prevails by a two-step energy transfer from Cy3 which in turn accepts energy from CdSe. Upon binding to maltose, the β-CD–Cy3.5 conjugate is displaced and, in the absence of the terminal acceptor, Cy3 is the predominant emitting species.

A hybrid NC–antibody that senses TNT operates by the mechanism shown in Fig. 3B.[38] In place of MBP, an anti-TNT specific antibody fragment is appended with an oligohistidine sequence, which is bound to the surface of a CdSe/ZnS NC. A TNT analogue pre-labeled with a quencher dye (Black Hole Quencher-10, BHQ-10) was pre-docked in the recognition site of the antibody. The docked dye quenches NC emission. The NC emission is ''turned-on'' when TNT displaces the quencher from the sensor, as shown in Fig. 4. The specificity of the TNT sensor was tested by comparing the effectiveness of FRET from the NC to the quencher dye for three different TNT analogues. The analyte specificity of the original antibody fragment was conserved after being bound to the NC. This approach is general and constructs involving an antibody fragment bound to a NC surface through noncovalent self-assembly should find wider use as a target of other analytes of interest.

3D: Sensing by NC-to-NC FRET

The NC–dye constructs incorporating analyte-displacement strategies are excellent single-response sensors. To realize maximum sensitivity and utility, however, a more ideal sensor would be reversible and/or self-referencing (or ratiometric). One such scheme is shown by Fig. 3D. FRET between small (green) and large (red) CdSe/ZnS nanocrystals has been implemented to sense potassium ions.[39] 15-crown-5 ethers were adsorbed onto the surface of the NCs through the bidentate thiol of dihydrolipoic acid. Prior to adding K^+ ions, both green and red NC emissions are present; the NC solutions were dilute enough to prevent energy transfer between the two NCs. Upon adding $KClO_4$, the green emission of the smaller NCs gradually decreased, while the red emission of the larger

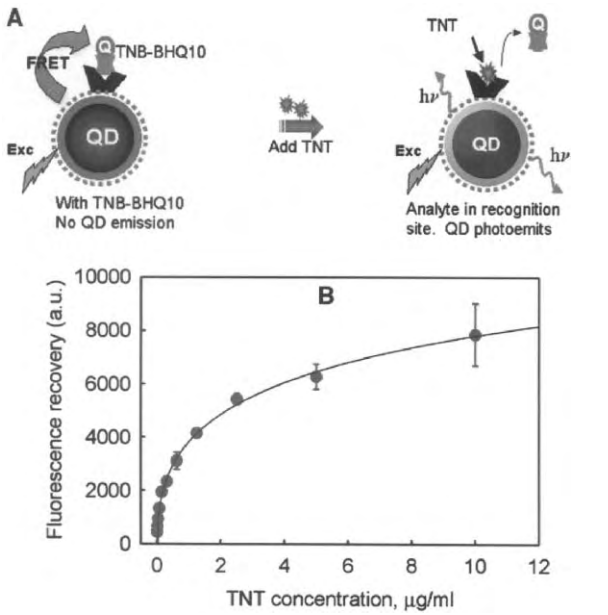

Fig. 4 (A) A schematic diagram of the quencher-displacement mechanism to sense TNT. (B) Increase in the NC photoluminescence *versus* concentration of TNT. (Reproduced with permission from *J. Am. Chem. Soc.*, 2005, **127**, 6744.[38] Copyright 2005 American Chemical Society.)

NCs increased. This synchronous change in emission intensities was ascribed to an energy transfer mechanism caused by aggregation of the NCs. The aggregate formed by the recognition of K^+ ions by the 15-crown-5 ethers to furnish a 15-crown-5–K^+–15-crown-5 sandwich complex. It was unclear whether the sandwich complex was formed from the coordination of two ether molecules from the neighboring arms of the same NC (intraparticle association) or from the two ether molecules of different NCs (interparticle association). A response was observed over a 10^{-6}–10^{-4} M concentration of $KClO_4$; the NCs were observed to precipitate from solution at higher $KClO_4$ concentrations. The sensing construct showed excellent sensitivity; however, high association between the K^+ ion and the crown ether as well as aggregation between the NCs at high concentrations makes reversible sensing difficult.

3E: Sensing by NC conjugation to analyte-sensitive chromophores

A reversible CdSe/ZnS NC sensor of pH operates according to Fig. 3E.[40] A pH-sensitive chromophore was conjugated to NC with a lipoic acid derivitized with a [1,3]oxazine ring. The [1,3]-oxazine ring may be opened by hydroxide anion to generate a 4-nitrophenylazophenolate chromophore. The absorption spectrum of this chromophore overlaps with the emission spectrum of the NC. This spectral overlap activates FRET, leading to a diminution of NC luminescence. Specifically, the NC emission intensity decreases by 35% over the pH from 7.1 to 8.5. The sole emission from the NC results in a detection signal that is not referenced, making calibration difficult.

3F: Sensing by NC conjugation to analyte-sensitive lumophores

In general, pH, or for that matter, the concentration of any analyte is difficult to quantify with a simple change in emission intensity of donor and/or acceptor. An accurate measurement of analyte concentration is unattainable if the overall background intensity changes, emission from species in the environment is present, or if the dye emission is sensitive to an interferent. These problems can be circumvented by constructing a reversible and ratiometric sensor according to the mechanism shown in Fig. 3F.

The construction of a CdSe/ZnS NC sensor of pH per Fig. 3F[41] was begun by encapsulating a CdSe/ZnS NC in an amphiphilic polymer in a similar manner as reported by Wu *et al.* to impart water solubility.[8] The polymer scaffold provides a hydroxy functionality for coupling organic molecules to the NC. Using 1-ethyl-3-(3-dimethylaminopropyl)-carbodiimide (EDC) coupling, a pH-sensitive squaraine dye was covalently attached *via* ester linkages. The absorption and the emission spectra of the squaraine dye are pH sensitive. The dye is highly absorptive and emissive at low to neutral pH. With increasing pH, the overall emission intensity decreases monotonically as shown in Fig. 5. The ratiometric nature of the sensor is derived from the modulation of the FRET efficiency arising from the engineered overlap of the pH-dependent squaraine dye absorption spectrum with the (pH-insensitive) NC emission spectrum. Upon excitation of the CdSe/ZnS NC, the NC may either fluoresce or transfer energy to the squaraine dye. At low pH, the overlap of the dye absorption spectrum and NC emission spectrum is small owing to the low absorption cross-section of the former. Under these conditions, FRET is efficient and the dye is more emissive than the NC owing to energy transfer. As the pH is raised, energy transfer from the NC to the dye is less efficient owing to poorer spectral overlap. The inset of Fig. 5 depicts the variation of the critical transfer distance (R_0) with solution pH due to the modulation of the overlap integral of eqn (3). The efficiency of the sensor is approximately a linear function of the modulation of the overlap of the NC and dye emission. Time-resolved fluorescence spectroscopy and excitation spectra provided further support for the energy transfer mechanism.

As a result of the FRET efficiency modulation, the emissions of the NC and dye were found to be naturally ratiometric. For a simple two-state system, with modulated energy transfer, an isosbestic point should be maintained in the photoluminescence spectrum. This is observed in Fig. 6. The relative emission intensities vary significantly with the largest changes occurring near the dye pK_a; an isosbestic point is maintained at 640 nm. The solution pH can be read out precisely by taking the ratio of emission peak intensities (NC and dye) to the intensity at the isosbestic point, which functions as an internal reference. This ratiometric approach is powerful when compared to typical CBsensors that display a single intensity-based response to analytes (*i.e.* either brightening or darkening) because the ratiometric construct is not sensitive to fluctuations of light excitation or collection efficiency as sensing is self-referencing. This is shown in Fig. 7. The pH may be determined accurately to 5% in highly scattering environments or when the excitation intensity is highly fluctuating. Such precision is impossible to achieve for the dye alone. In addition, the continuous absorption manifold of the CdSe NCs results in an excitation-wavelength independent bandshape, a feature that is not present in single molecular ratiometric sensors. Thus, the NC–dye conjugate does not need to use two independent excitation sources (or alternatively a single excitation specifically at an absorptive isosbestic point) for proper function. The approach is completely general for any analyte that modulates FRET involving the NC. The reversible and ratiometric nature of the approach presented by Fig. 3F makes NCs versatile agents for chemical and biological sensing.

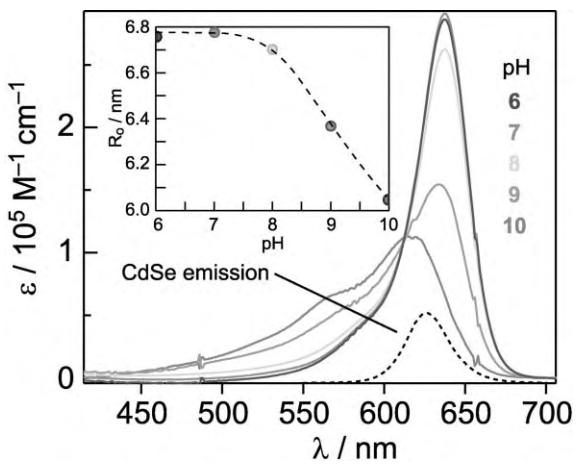

Fig. 5 The pH-dependent absorption profile of a squaraine dye overlaid with the emission of the CdSe/ZnS NC. The inset depicts the variation of the critical transfer distance due to the modulation of the spectral overlap integral by solution pH.

CdSe as gain material in lasing cavities

The physical properties and dimensions of NCs naturally lend them to sensing on small length scales. On this count, NCs have a significant advantage over conventional molecular chemosensors. Owing to their photostability and spectrally narrow gain profiles, NCs can function as gain materials for

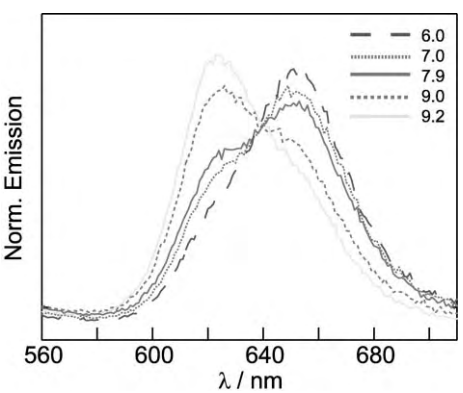

Fig. 6 Emission spectra of the NC–squaraine dye construct at different pH. The isosbestic point at 640 nm allows for ratiometric sensing.

laser cavities on micro-dimensions.[42] The ability to amplify NC output signals in such cavities offers unique opportunities for detecting the signal from NC sensor constructs on small length scales.

As CBsensing is scaled down, the number of receptor sites decreases on a sensing platform. Device sensitivity and performance is compromised because the optical sensing mechanism of typical chemosensors, single molecule detection–single photon generation, yields signals that are too weak to be detected. In principle, the linear, single photon response of a molecular chemosensor can be replaced with the non-linear one of a NC that is part of a laser cavity (see Fig. 8). An example of this sensing strategy with TNT-sensing semiconducting organic polymer as gain material has already been reported by Rose *et al.*; enhanced sensitivity to TNT was found to be most pronounced when the polymer-incorporated distributed feedback films were pumped at intensities near their lasing threshold, exhibiting non-linear sensing.[43] Because the NCs are robust, they can withstand the high fields generated in such cavities. This review concludes with a discussion of lasing cavities incorporating NCs and their potential for high gain CB sensing.

Theory and motivation on high gain sensing

The intensity of light can build exponentially as light propagates in a cavity with an inverted excited state population. This exponential increase in intensity is given by,[14]

$$I = I_0 e^{g(v)z} \tag{5}$$

where I_0 is the seed intensity, I is the intensity at some distance z into the cavity, and $g(v)$ is the gain coefficient given by eqn (6).

$$g(v) = [N_u B_u(v) - N_l B_l(v)] \frac{hv}{c} \tag{6}$$

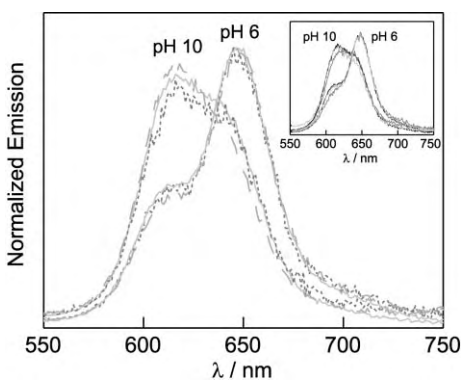

Fig. 7 Sensing of the local pH by the NC–squaraine dye construct with variations in the excitation intensity and local environment. The ratio of NC to dye emission varies such that pH is determined within 5% when altering the slit entrance of the Xe lamp excitation of the fluorimeter (--- 0.5 mm; —, 2.00 mm) and when examining the construct within a highly scattering media, which consisted of a solution of silica microspheres (— —). The inset shows that emission was independent of excitation wavelength (—, 380 nm; —, 450 nm; —, 520 nm).

where N_u and N_l are the upper and lower level populations, respectively, and $B_u(v)$ and $B_l(v)$ are the emission and absorption probability, respectively, at frequency v. Separation of Einstein B_u and B_l coefficients from the population inversion allows eqn (5) to be recast as,

$$I = I_0 e^{\sigma(v)\Delta N_{ul}z} \tag{7}$$

where $\sigma(v)$ is the stimulated emission cross-section. Eqn (7) provides an immediate inroad to sensing. If an analyte can affect the photophysics of the NC by removing or adding energy to the cavity (in a FRET process or by another signal transduction mechanism), the gain coefficient will be perturbed, leading to an exponential change in the laser output. A non-linear, highly sensitive "turn-off" or "turn-on" sensor can potentially be made.

High intensities and maximal response from the laser cavity can most easily be achieved by confining light within the cavity of the laser resonator. In a conventional Fabry-Perot resonator, confinement is achieved by reflection of light off a front and back mirror. With CdSe NCs as gain materials, Distributed Feedback (DFB) and spherical Whispering Gallery Mode (WGM) cavities (see Fig. 9) have been used to confine light to obtain lasing devices.[44–48]

CdSe incorporated DFBs

Optical gain and stimulated emission using CdSe NCs at room temperature was reported by Klimov *et al.*[42] In this work, gain-induced narrowing of the fluorescence emission spectrum (or amplified spontaneous emission, ASE) was achieved in close-packed drop-cast films of NCs. In order to achieve ASE, high volume fractions of NCs as well as ultrafast optical pumping (100 fs pulses) were shown to be essential in overcoming competitive nonradiative processes. With the parameters to achieve gain in NC films defined, the chemistry needed to incorporate them into feedback structures to attain lasing was developed.[44,45]

The architecture of a second-order DFB comprises a slab waveguide imprinted with a grating of period (Λ) that satisfies the Bragg condition,

$$\Lambda = \frac{\lambda_B m}{2n_{eff}} \tag{8}$$

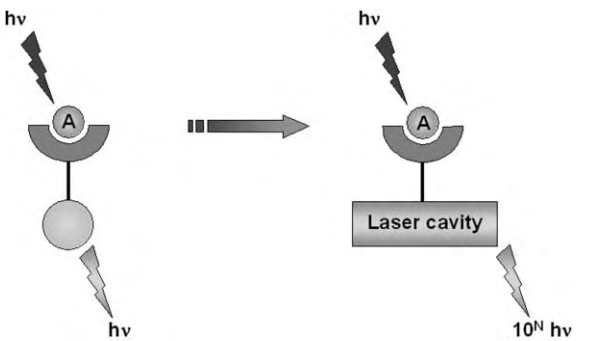

Fig. 8 Design concept to achieve CB sensing on small lengths scales. A single photon emitting center is replaced by a laser, which can be turned off or on by the recognition of a target. The strategy allows for high gain responses in the presence of analyte at low concentrations.

where λ_B is the Bragg wavelength that is supported by period Λ, m is the order of the grating reflection, and n_{eff} is the effective refractive index.[14] The lasing medium must have a gain profile that is coincident with λ_B. Stimulated emission of light is achieved as the propagating wave traverses the DFB grating and builds up gain from the constructive feedback caused by the grating.

Eisler *et al.* encapsulated CdSe NCs within feedback structures by spin coating a NC–titania thin film on top of a DFB grating; the grating was generated using interference holography and patterned onto a silica wafer through reactive-ion-etching (RIE).[44] The thickness of the film was controlled by the speed of the spin coating, and the volume fraction of the NCs, which controls the refractive index. As defined by eqn (8), n_{eff} was adjusted to match the Bragg condition of the grating for the given ASE of the NC–titania film. Using different size NCs, different DFB lasers were produced over a wavelength range from 560 nm to 625 nm. The technology was further expanded by embossing a DFB pattern directly onto the NC–titania thin film.[45] In this work, a poly(dimethylsiloxane) (PDMS) elastomeric stamp was patterned with a DFB grating, brought into contact with a freshly spin-coated NC–titania pre-polymer, which was transferred to a hot plate to initiate polymerization. The pattern of the PDMS stamp is preserved upon polymerization and lasing, as shown in Fig. 10, is achieved. Soft lithography allows multilayer structures to be prepared by overlaying DFB gratings of different periodicity (and accordingly different sized NCs). With a multi-layered DFB laser, simultaneous lasing of multiple colors may be observed.

The sol–gel derived NC–titania films of Fig. 10 degrade rapidly after exposure to water and short chain alcohols. Recent work by Chan *et al.* describes the development of a solvent stable NC–silica composite laser.[48] CdSe/ZnS NCs were modified with 5-amino-1-pentanol to impart ethanol solubility. The silica precursors were 3-aminopropyltrimethoxy-silane and (triethoxysilyl)propyl isocyanate were added to the NC–ethanol solution. The film fabrication and grating pattern transfer were performed in the same manner as described above to yield a device that was stable in several solvents. Stable lasing was observed from these DFBs in the presence of water as well as short-chain alcohols. These results enable NC-based DFBs to be used for high gain sensing in aqueous environments.

CdSe incorporated spherical resonators

Lasing from NCs can also be achieved in spherical cavities that support Whispering Gallery Modes (WGM). The WGM is formed from the constructive interference of successive total internal reflections of light off the concave inner surface of the spherical cavity.[14] Due to the strong confinement of photons within the modal volume, the laser Q-factor of these modes can be as high as 10^8.[14] CdSe/ZnS NCs are particularly suited to spherical resonators because they can withstand the high power densities that are developed within the small volume of the microsphere.

WGM lasing structures may be fabricated by assembling thin films of CdSe NCs onto 10 μm polystyrene spheres using a layer-by-layer wet chemical procedure; however, the highly

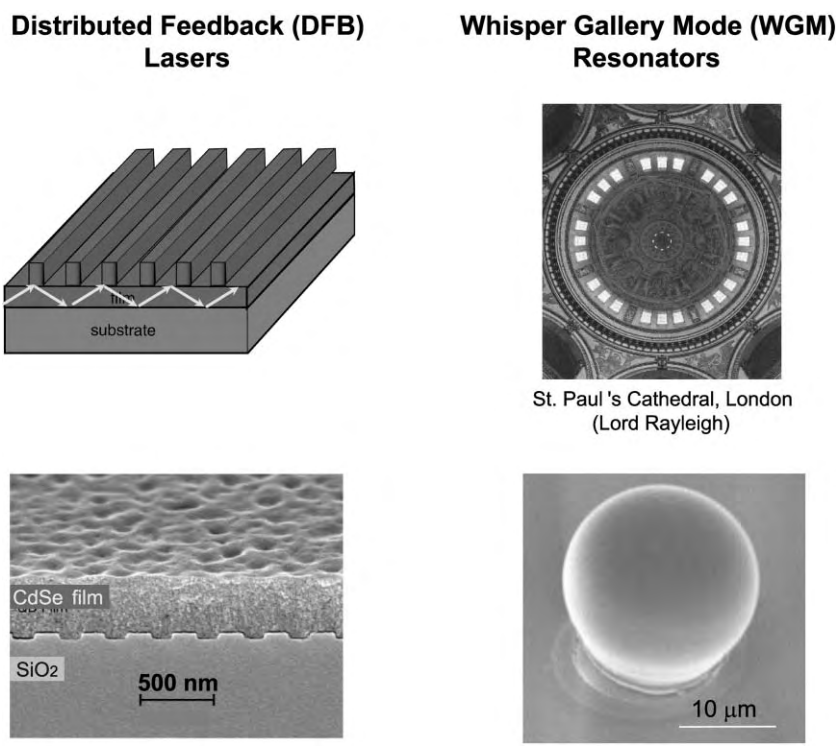

Fig. 9 Two different types of laser cavities incorporating CdSe NCs as gain media. (A) Schematic representation of a distributed feedback (DFB) grating and a SEM image of the grating. (B) The reflection of sound waves that can be found at the Whispering Gallery of the St. Paul's Cathedral in London can be adapted on a smaller length scale to trap light waves in a spherical microcavity. An SEM of a NC-coated microsphere is shown.

loaded fraction of NCs that is necessary for light amplification is difficult to achieve by this method.[46]

Kazes *et al.* reported lasing from CdSe/ZnS NCs and quantum rods by using a cylindrical microcavity constructed from an optical fiber within a glass capillary tube.[49] A solution of the NCs or the quantum rods filled the space between the fiber and the capillary tube. The microcavity was pumped with a nanosecond Nd-YAG laser. The lasing threshold for the NC microcavity was 3 mJ whereas the threshold of the quantum rod microcavity was at 0.08 mJ. The linearly polarized emission of the CdSe quantum rods was observed from the lasing microcavity. Along similar lines, Petruska *et al.*[50] incorporated the matrix formed from NCs tethered to a titania sol–gel matrix by using alcohol-terminating amines into glass microcapillary tubes to promote WGM resonance. Lasing was obtained at room-temperature using a femtosecond excitation source.

Snee *et al.* developed a facile method of incorporating NCs onto the surface of micron-sized silica or polystyrene microspheres to produce a lasing cavity that is both reproducible and stable.[46] This synthetic methodology entails mixing a NC–titania sol precursor with silica microspheres before spin casting onto a glass substrate and annealing at high temperature (see Fig. 11). The disparity in the size of the titania film and the microsphere feedstock results in a conformal coating of the titania film onto the microspheres. Fig. 12 shows the lasing obtained from these WGM resonator composites. A clear threshold is observed for biexcitonic lasing on the low energy side of the quantum dot fluorescence. The facile and robust method of incorporating NCs as gain material for spherical resonators was found to be general;

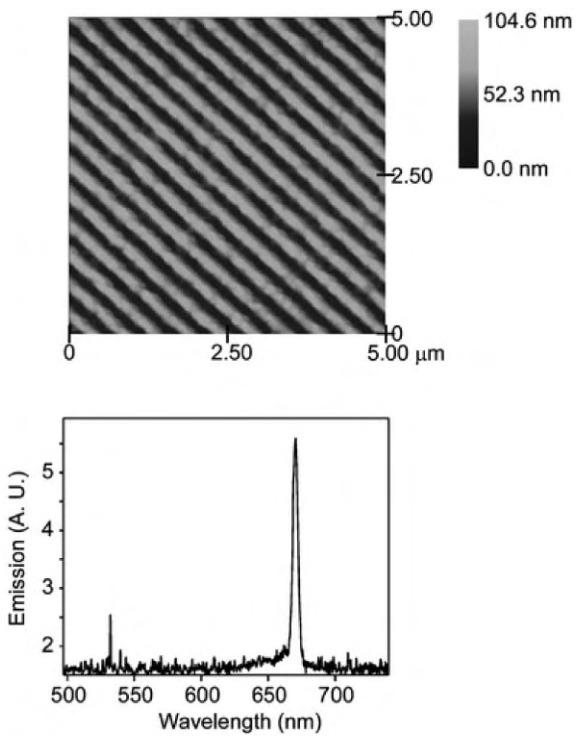

Fig. 10 (Top) AFM of NCs incorporated into a thin film. (Bottom) The emission spectrum of a NC-titania DFB laser device. (Reproduced from *J. Mater. Chem.*, 2005, **15**, 2697.[14])

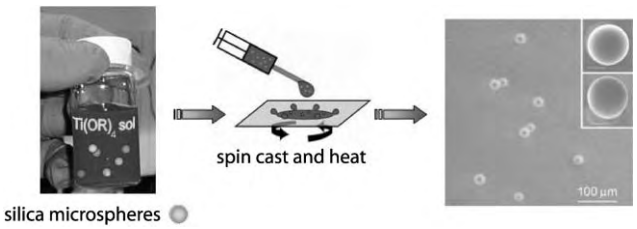

Fig. 11 A schematic representation for the synthesis of NC coated microspheres to produce a NC-microsphere that exhibits lasing from a whisper gallery mode. The silica microspheres are on the order of microns; their size is exaggerated in the container on the left in order to emphasize the nature of the synthetic procedure.

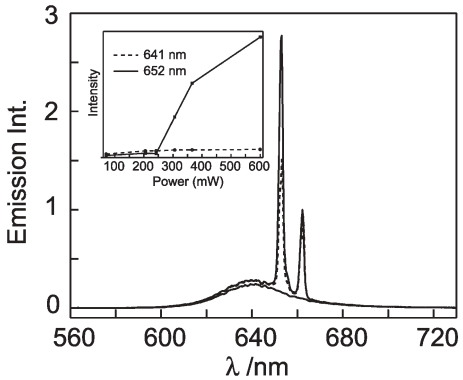

Fig. 12 Fluorescence from the CdSe NCs (bottom trace) transforms into discrete sharp lines once the lasing threshold is crossed. Inset shows the non-linear increase in intensity at threshold pump intensity at 652 nm while the fluorescence at 641 nm shows a linear response.

different NCs can be used to achieve lasing at different wavelengths,[47] and WGM resonant cavity structures can be introduced using a variety of commercially available microsphere templates.[46] The overcoating of NC–titania sols onto the spheres produces hundreds of uniform microresonators in a single spin-coating process, which opens up the potential for multiplexed sensing modalities.

Prospects for non-linear sensing using CdSe as gain material

The development of environmentally responsive CdSe NC constructs, together with NC-based DFB thin film and WGM spherical lasing platforms, opens the way for the development of high gain CBsensors. The gain coefficient of NC-based laser cavities may be altered through the modulation of energy transfer by the various mechanisms shown in Fig. 3. The excited state population may be reduced through resonance energy transfer loss channels. Consequently, the loss of the excited state concentration (decrease in ΔN_{ul}) will represent a significant portion of the total population inversion resulting in a large change in the amplified laser intensity. When the loss of energy within the laser cavity is greater than the gain, the laser turns off, which can then be easily observed. Alternatively, the energy transfer mechanisms may be constructed to enhance the excited state population through excitation of the NC by the analyte. In either of these strategies, the response of the analyte by the NC is perturbed

in a highly non-linear fashion, thereby facilitating signal detection. Alternatively, the surface of CdSe NCs, which are part of a lasing cavity, are amenable to modification with receptor sites. Recognition of target analytes that absorb or emit at the propagating frequency can in principle add to the gain or loss mechanism.

The ability to produce very high Q laser cavities using standard sol–gel chemistry offers other opportunities for highly non-linear sensing. The optical Q factor is proportional to the timescale that energy is stored in the cavity compared to the rate of energy loss. Consequently, higher Q cavities have longer photon storage times, increasing the effective length scale over which the laser light is amplified. The change in intensity and sensitivity as a result of the loss or gain of excited state population is exponential with respect to the length scale of laser light amplification. Additional sensitivity may be achieved by the direct modification of the Q factor itself, which will shift the wavelengths of lasing emission. The wavelengths of DFB and WGM, lasing emission lines are very sensitive to the refractive index of the gain medium. Adsorption of an analyte on the surface of the lasing device has the potential of altering the Q-factor and changing the optical properties of the structure, which would change the lasing wavelength. Because the laser lines are narrow, the shift in the lasing wavelength can be monitored easily.

Summary

The attractive properties of broad absorption profiles, narrow tunable emissions, high photostability, and high quantum yields for NCs have led to their development as CBsensors. The narrow emissions of the NCs as well as their resistance to photobleaching compared to those of organic dyes hold promise for multiplexing applications in a biological environment. In addition, the development towards self-calibrating NC sensors has expanded the utility of NC biosensors to be comparable to that of organic dyes. For sensing, as opposed to imaging, the NC photophysics must be sensitive to their environment. Most applications to date have focused on utilizing FRET as the mechanism to perturb the photophysics. However, other mechanisms exist. A recent report by Sykora *et al.* has demonstrated that CdSe emission is completely quenched by carboxylated Ru–polypyridyl complexes.[51] This result, accompanied by the fact that the spectral overlap is small, suggests charge transfer as the predominant mechanism for NC quenching as opposed to FRET. Considering the effectiveness of electron transfer as an excited state quenching mechanism, the development of NC CBsensors whose signal transduction is derived from charge transfer appears to be a particularly fruitful line of inquiry.[52] Finally, the use of NCs as gain materials in lasing cavities lays the foundation for non-linear sensing strategies that allow for the rapid and ultrasensitive detection of target analytes by NC-based CBsensors.

Acknowledgements

R.C.S. would like to thank Dr P. T. Snee and Dr A. B. Greytak for helpful discussions. R.C.S. also thanks the Corning Foundation for a graduate fellowship. We acknowledge sustained support from the National Science Foundation through the Collaborative Research in Chemistry program (CHE-0209898) and the Army Research Office (W911NF-06-1-0101) for support of the basic research needed to unify CB sensing and NCs.

References

1 C. B. Murray, D. J. Norris and M. G. Bawendi, *J. Am. Chem. Soc.*, 1993, **115**, 8706.
2 M. A. Hines and P. Guyot-Sionnest, *J. Phys. Chem.*, 1996, **100**, 468.
3 B. O. Dabbousi, J. Rodriguez-Viejo, F. V. Mikulec, J. R. Heine, H. Mattoussi, R. Ober, K. F. Jensen and M. G. Bawendi, *J. Phys. Chem. B*, 1997, **101**, 9463.
4 J. K. Jaiswal and S. M. Simon, *Trends Cell Biol.*, 2004, **14**, 497 and all references therein.
5 M. Bruchez, M. Moronne, P. Gin, S. Weiss and A. P. Alivisatos, *Science*, 1998, **281**, 2013.
6 W. C. W. Chan and S. Nie, *Science*, 1998, **281**, 2016.
7 B. Dubertret, P. Skourides, D. J. Norris, V. Noireaux, A. H. Brivanlou and A. Libchaber, *Science*, 2002, **298**, 1759.
8 X. Wu, H. Liu, J. Liu, K. N. Haley, J. A. Treadway, J. P. Larson, N. Ge, F. Peale and M. P. Bruchez, *Nat. Biotechnol.*, 2003, **21**, 41.
9 W. Guo, J. J. Li, Y. A. Wang and X. Peng, *Chem. Mater.*, 2003, **15**, 3125.
10 S. Kim and M. G. Bawendi, *J. Am. Chem. Soc.*, 2003, **125**, 14652.
11 I. L. Medintz, H. T. Uyeda and E. R. Goldman, *Nat. Mater.*, 2005, **4**, 435.
12 J. Aldana, Y. A. Wang and X. Peng, *J. Am. Chem. Soc.*, 2001, **123**, 8844.
13 A. M. Derfus, W. C. W. Chan and S. N. Bhatia, *Nano Lett.*, 2004, **4**, 11.
14 A. W. Wun, P. T. Snee, Y. T. Chan, M. G. Bawendi and D. G. Nocera, *J. Mater. Chem.*, 2005, **15**, 2697 and all references therein.
15 G. W. Walker, V. C. Sundar, C. M. Rudzinski, A. W. Wun, M. G. Bawendi and D. G. Nocera, *Appl. Phys. Lett.*, 2003, **83**, 3555.
16 H. Hu, M. M. Koochesfahani, B. Shafii, P. T. Snee, M. G. Bawendi and D. G. Nocera, *Bull. Am. Phys. Soc.*, 2005, **50**, 167.
17 S. Pouya, M. M. Koochesfahani, P. T. Snee, M. G. Bawendi and D. G. Nocera, *Exp. Fluids*, 2005, **39**, 784.
18 D. H. Son, S. M. Hughes, Y. Yin and A. P. Alivisatos, *Science*, 2004, **306**, 1009.
19 J. Lee, A. O. Govorov and N. A. Kotov, *Nano Lett.*, 2005, **5**, 2063.
20 J. R. Lakowicz, *Principles of Fluorescence Spectroscopy,* Kluwer Academic Publishers, New York, 2nd edn, 1999.
21 A. R. Clapp, I. L. Medintz, J. M. Mauro, B. R. Fisher, M. G. Bawendi and H. Mattoussi, *J. Am. Chem. Soc.*, 2004, **126**, 301.
22 C. R. Kagan, C. B. Murray, M. Nirmal and M. G. Bawendi, *Phys. Rev. Lett.*, 1996, **76**, 1517.
23 R. Wargnier, A. V. Baranov, V. G. Maslov, V. Stsiapura, M. Artemyev, M. Pluot, A. Sukhanova and I. Nabiev, *Nano Lett.*, 2004, **4**, 451.
24 (*a*) D. M. Willard, L. L. Carillo, J. Jung and A. Van Orden, *Nano Lett.*, 2001, **1**, 469; (*b*) D. M. Willard, L. L. Carillo, J. Jung and A. Van Orden, *Nano Lett.*, 2001, **1**, 581.
25 P. T. Tran, E. R. Goldman, G. P. Anderson, J. M. Mauro and H. Mattoussi, *Phys. Status Solidi B*, 2002, **229**, 427.
26 S. Hohng and T. Ha, *ChemPhysChem*, 2005, **6**, 956.
27 D. Zhou, J. D. Piper, C. Abell, D. Klenerman, D.-J. Kang and L. Ying, *Chem. Commun.*, 2005, 4807.
28 A. R. Clapp, I. L. Medintz, B. R. Fisher, G. P. Anderson and H. Mattoussi, *J. Am. Chem. Soc.*, 2005, **127**, 1242.
29 M. Achermann, M. A. Petruska, S. Kos, D. L. Smith, D. D. Koleske and V. I. Klimov, *Nature*, 2004, **429**, 642.
30 M. Anni, L. Manna, R. Cingolani, D. Valerini, A. Creti and M. Lomascolo, *Appl. Phys. Lett.*, 2004, **85**, 4169.
31 N. Hildebrandt, L. J. Charbonnière, M. Beck, R. F. Ziessel and H.-G. Löhmannsröben, *Angew. Chem., Int. Ed.*, 2005, **44**, 7612.

32 P. O. Anikeeva, C. F. Madigan, S. A. Coe-Sullivan, J. S. Steckel, M. G. Bawendi and V. Bulovic, *Chem. Phys. Lett.*, 2006, **424**, 120.
33 F. Patolsky, R. Gill, Y. Weizmann, T. Mokari, U. Banin and I. Willner, *J. Am. Chem. Soc.*, 2003, **125**, 13918.
34 R. Gill, I. Willner, I. Shweky and U. Banin, *J. Phys. Chem. B*, 2005, **109**, 23715.
35 R. Bakalova, Z. Zhelev, H. Ohba and Y. Baba, *J. Am. Chem. Soc.*, 2005, **127**, 11328.
36 C.-Y. Zhang and L. W. Johnson, *J. Am. Chem. Soc.*, 2006, **128**, 5324.
37 I. L. Medintz, A. R. Clapp, H. Mattoussi, E. R. Goldman, B. Fisher and J. M. Mauro, *Nat. Mater.*, 2003, **2**, 630.
38 E. R. Goldman, I. L. Medintz, J. L. Whitley, A. Hayhurst, A. R. Clapp, H. T. Uyeda, J. R. Deschamps, M. E. Lassman and H. Mattoussi, *J. Am. Chem. Soc.*, 2005, **127**, 6744.
39 C.-Y. Chen, C.-T. Cheng, C.-W. Lai, P.-W. Wu, K.-C. Wu, P.-T. Chou, Y.-H. Chou and H.-T. Chiu, *Chem. Commun.*, 2006, 263.
40 M. Tomasulo, I. Yildiz and F. M. Raymo, *J. Phys. Chem. B*, 2006, **110**, 3853.
41 P. T. Snee, R. C. Somers, J. Zimmer, G. Nair, M. G. Bawendi and D. G. Nocera, *J. Am. Chem. Soc.*, 2006, **128**, 13320.
42 V. I. Klimov, A. A. Mikhailovsky, S. Xu, A. Malko, J. A. Hollingsworth, C. A. Leatherdale, H.-J. Eisler and M. G. Bawendi, *Science*, 2000, **290**, 314.
43 A. Rose, Z. Zhu, C. F. Madigan, T. M. Swager and V. Bulovic, *Nature*, 2005, **434**, 876.
44 H.-J. Eisler, V. C. Sundar, M. G. Bawendi, M. Walsh, H. I. Smith and V. Klimov, *Appl. Phys. Lett.*, 2002, **80**, 4614.
45 V. C. Sundar, H.-J. Eisler, T. Deng, Y.-T. Chan, E. L. Thomas and M. G. Bawendi, *Adv. Mater.*, 2004, **16**, 2137.
46 P. T. Snee, Y. Chan, D. G. Nocera and M. G. Bawendi, *Adv. Mater.*, 2005, **17**, 1131.
47 Y. Chan, J. S. Steckel, P. T. Snee, J.-M. Caruge, J. M. Hodgkiss, D. G. Nocera and M. G. Bawendi, *Appl. Phys. Lett.*, 2005, **86**, 073102.
48 Y. Chan, P. T. Snee, J.-M. Caruge, B. K. Yen, G. Nair, D. G. Nocera and M. G. Bawendi, *J. Am. Chem. Soc.*, 2006, **128**, 3146.
49 M. Kazes, D. Y. Lewis, Y. Ebenstein, T. Mokari and U. Banin, *Adv. Mater.*, 2002, **14**, 317.
50 M. A. Petruska, A. V. Malko, P. M. Voyles and V. I. Klimov, *Adv. Mater.*, 2003, **15**, 610.
51 M. Sykora, M. A. Petruska, J. Alstrum-Acevedo, I. Bezel, T. J. Meyer and V. I. Klimov, *J. Am. Chem. Soc.*, 2006, **128**, 9984.
52 M. G. Sandros, D. Gao and D. E. Benson, *J. Am. Chem. Soc.*, 2005, **127**, 2198.